## ARTICLE

# Megakaryopoiesis impairment through acute innate immune signaling activation by azacitidine

Ujunwa Cynthia Okoye-Okafor[1,2], Komal K. Javarappa[3]*, Dimitrios Tsallos[3]*, Joseph Saad[3]*, Daozheng Yang[1], Chi Zhang[1], Lumie Benard[1,2], Victor J. Thiruthuvanathan[1,2], Sally Cole[1,2], Stephen Ruiz[1,2], Madhuri Tatiparthy[1,2], Gaurav Choudhary[5], Stefanie DeFronzo[1], Boris A. Bartholdy[1], Celine Pallaud[4], Pedro Marques Ramos[4], Aditi Shastri[5], Amit Verma[5], Caroline A. Heckman[3], and Britta Will[1,2,5]

**Thrombocytopenia, prevalent in the majority of patients with myeloid malignancies, such as myelodysplastic syndrome (MDS) or acute myeloid leukemia (AML), is an independent adverse prognostic factor. Azacitidine (AZA), a mainstay therapeutic agent for stem cell transplant–ineligible patients with MDS/AML, often transiently induces or further aggravates disease-associated thrombocytopenia by an unknown mechanism. Here, we uncover the critical role of an acute type-I interferon (IFN-I) signaling activation in suppressing megakaryopoiesis in AZA-mediated thrombocytopenia. We demonstrate that megakaryocytic lineage-primed progenitors present IFN-I receptors and, upon AZA exposure, engage STAT1/SOCS1-dependent downstream signaling prematurely attenuating thrombopoietin receptor (TPO-R) signaling and constraining megakaryocytic progenitor cell growth and differentiation following TPO-R stimulation. Our findings directly implicate RNA demethylation and IFN-I signal activation as a root cause for AZA-mediated thrombocytopenia and suggest mitigation of TPO-R inhibitory innate immune signaling as a suitable therapeutic strategy to support platelet production, particularly during the early phases of AZA therapy.**

## Introduction

Myelodysplastic syndrome (MDS) and acute myeloid leukemia (AML) are hallmarked by ineffective hematopoiesis, generation of dysfunctional myeloid cells, and single or multi-lineage cytopenia, including thrombocytopenia (Will et al., 2012).

The cytosine analog and DNA hypomethylating agent (HMA) azacitidine (AZA) is one of the current therapies for MDS and is used in AML for individuals who are ineligible for stem cell transplantation or high-dose myeloablative chemotherapy (Fenaux et al., 2009, National Comprehensive Cancer Network, 2017). While this cytosine analog effectively reverses disease-associated DNA methylation and alleviates dysregulated myeloid differentiation, it is not curative (Christman et al., 1983). Its clinical application is largely limited by its bone marrow (BM)–suppressive effects, including neutropenia and thrombocytopenia (Kantarjian et al., 2007; Aparicio and Weber, 2002). How AZA elicits these inhibitory effects has remained incompletely unsolved, hindering its effective use as an anti-leukemic therapy, particularly in MDS/AML.

Thrombocytopenia, platelet (PLT) counts of $<100 \times 10^9$/liter, occurs in 40–65% of patients with MDS (Neukirchen et al.,

2009). It can increase the risk of bleeding and hampers the effective clinical management of patients as it necessitates the discontinuation of anti-leukemic treatment (Webb and Anderson, 1999). Low PLT counts are an independent prognostic factor and have been included in clinical classification systems (de Swart et al., 2015). The capacity to generate PLTs during primary disease and early after anti-leukemic therapy appears to be reflective of patients' non-leukemic cell reserve and BM function and is highly associated with successful therapeutic intervention (van den Bosch et al., 2004). Thus, supporting efficient megakaryopoiesis and PLT generation are highly important clinical priorities in the management and treatment of MDS/AML. PLT transfusions have long been the primary therapeutic option for clinically significant thrombocytopenia (McCullough, 2000); albeit, they are only effective short-term as they increase the risk of alloimmunization (Reckhaus et al., 2018; Webb and Anderson, 1999).

Steady-state PLT production from megakaryocytes is governed primarily by thrombopoietin (TPO) and its receptor (TPO-R;

encoded by the myeloproliferative leukemia virus oncogene [cMPL]; Yu and Cantor, 2012). TPO ensures adequate megakaryocyte numbers (de Sauvage et al., 1996; Kaushansky, 2005). Highly potent TPO-R agonists (TPO-RA), eltrombopag (EP; Erickson-Miller et al., 2009) and romiplostim, have been clinically explored to counteract disease and HMA treatment-associated thrombocytopenia (Kuter, 2009; Wang et al., 2004). Despite several encouraging phase I/II trials in MDS and AML testing EP as a single agent or along with conventional therapy (Olnes et al., 2012; Svensson et al., 2014), the TPO-R mimetic failed to enhance PLT production in patients during early stages of AZA therapy (Dickinson et al., 2018).

No study has clarified the molecular pathogenesis of HMA-induced thrombocytopenia yet, but this will be essential to develop effective therapeutic strategies in mitigating AZA-induced thrombocytopenia. Our findings delineate the molecular and functional consequences of AZA in megakaryocytic (Mk) progenitors and provide a preclinical rationale for evaluating p38 MAPK inhibitors for increasing PLT in patients in the early stages of AZA therapy.

## Results

### AZA inhibits Mk progenitor growth and differentiation
To determine the effects of AZA on megakaryopoiesis, we characterized ex vivo Mk progenitor cell growth and differentiation of mononuclear cells (MNC) derived from healthy individuals or patients with MDS or AML (MDS/AML; Table S1) in the presence of a clinically relevant (Roulois et al., 2015) but non-cytotoxic dose of AZA (0.3 μM; Fig. 1 A and Fig. S1 A). Compared with vehicle controls, AZA treatment specifically inhibited immature and mature colony-forming Mk progenitor cell growth of healthy (Fig. 1 B) or MDS/AML MNC (Fig. 1 C) upon TPO-R stimulation with TPO-RA EP, or recombinant human TPO irrespective of TPO-RA dosage (Fig. S1, B–F). AZA also impaired the expansion of MNC in megakaryopoiesis-inducing cultures (Fig. 1, D and E; and Fig. S1, G–I) and decreased megakaryocyte-specific integrin CD41 (Haas et al., 2015) expression compared with vehicle-treated controls (Fig. 1 F), which was not attributable to the reduced presentation of Mk cell surface markers at the single cell level (Fig. S1, I–L). We found a 20% decrease in cells with clear morphological signs of Mk differentiation (increased cell size, multi-lobulated nucleus, and a lower cytosol/nucleus ratio) in AZA-treated cultures compared with controls (Fig. 1 G). Assessment of DNA content (increasing upon Mk cell maturation; Mattia et al., 2002) revealed a 30% increase in the number of diploid cells and a concomitant decrease in polyploid cells exposed to AZA compared with controls (Fig. 1 H and Fig. S1 M). We observed a decrease in the number of PLTs produced upon AZA treatment (Fig. 1 I and Fig. S1, N and O). Decitabine (DEC) showed similar megakaryopoiesis inhibitory effects (Fig. S1, P and Q). These data support that AZA inhibits Mk progenitor expansion, differentiation, and PLT production upon TPO-R stimulation, which may be common to chemical cytidine analogs.

### Suppression of Mk gene expression programs and activation of type-I IFN (IFN-I)–responsive genes by AZA
Characterization of gene expression changes in FACS-sorted primary MPL presenting cells upon acute AZA exposure (16 h; Fig. 2 A and Table S1) under megakaryopoiesis-promoting conditions revealed a substantial number of genes to be differentially expressed (Fig. 2, B–D; and Table S2) compared with mock-treated controls. We found a prevalence of myeloid gene expression signatures at the expense of Mk-erythroid progenitor cell programs (Fig. 2 E and Table S3) and activation of IFN-I responsive genes (Fig. 2, F and G; and Table S4).

Additionally, analysis of differentially expressed genes in paired BM-MNC (BM-MNC) specimens from patients before (pre-AZA) and following long-term treatment with AZA (post-AZA) in vivo (Fig. 2 H and Table S5) also showed a strong enrichment of transcripts associated with the negative regulation of Mk differentiation and activation of IFNα response genes (Fig. 2, I and J; and Tables. S6 and S7) in post-AZA specimen compared with their treatment naive counterparts, a finding which was recapitulated in an unrelated published gene expression set (Fig. 2 K).

These molecular alterations strongly suggested that AZA suppresses Mk differentiation programs in TPO-R presenting stem and progenitor cells and further indicated that AZA and DEC may activate innate immune signaling more rapidly than previously appreciated (Chiappinelli et al., 2015; Li et al., 2014; Roulois et al., 2015; Stone et al., 2017).

### AZA rapidly triggers innate immune pathway activation in Mk cells
RNA hypomethylation following AZA treatment has been described previously (Cheng et al., 2018; Schaefer et al., 2009). As the loss of methylation can increase the formation of immunogenic double-stranded RNA (dsRNA) species (Lee et al., 2019; Schaefer et al., 2009), we tested AZA's effects on total RNA cytosine methylation and dsRNA abundance. Following ex vivo stimulation of megakaryopoiesis using TPO-RA, AZA led to a rapid and transient decrease in global RNA 5-methylcytosine (5 mC) levels (Fig. 3, A–C and Fig. S2 A). Concomitantly, AZA exposure resulted in increased dsRNA levels within only 1 h in healthy and MDS/AML MNC (Fig. 3, D–F), as well as purified immature CD34+ hematopoietic stem and progenitor cells (HSPCs; Fig. S2, B–E). DEC treatment decreased total RNA 5-methyl cytosine marks (Fig. S2 F) and rapidly induced dsRNA accumulation in a dose-dependent manner (Fig. S2, G and H). This demonstrates that AZA triggers RNA hypomethylation independent of its ability to integrate into RNA.

RNA sensors, such as endosomal membrane-associated toll-like receptor 3 (TLR3) and the cytosolic MDA5/MAVS complex, activate innate immune pathways upon binding of immunogenic RNA species (Chiappinelli et al., 2015; Gantier and Williams, 2007). Consistently, we found increased levels of TLR3 in total MNC as well as purified HSPC within 1 h of AZA exposure (Fig. 3, G and H). MDA5 and MAVS mRNA were also found to increase upon treatment with AZA (Fig. S2, I and J). Upon a 24-h exposure to AZA and compared with mock controls, we observed increased MDA5 protein levels (Fig. 3 I) which

Okoye-Okafor et al.
Mitigating azacitidine-mediated thrombocytopenia

Journal of Experimental Medicine    2 of 17
https://doi.org/10.1084/jem.20212228
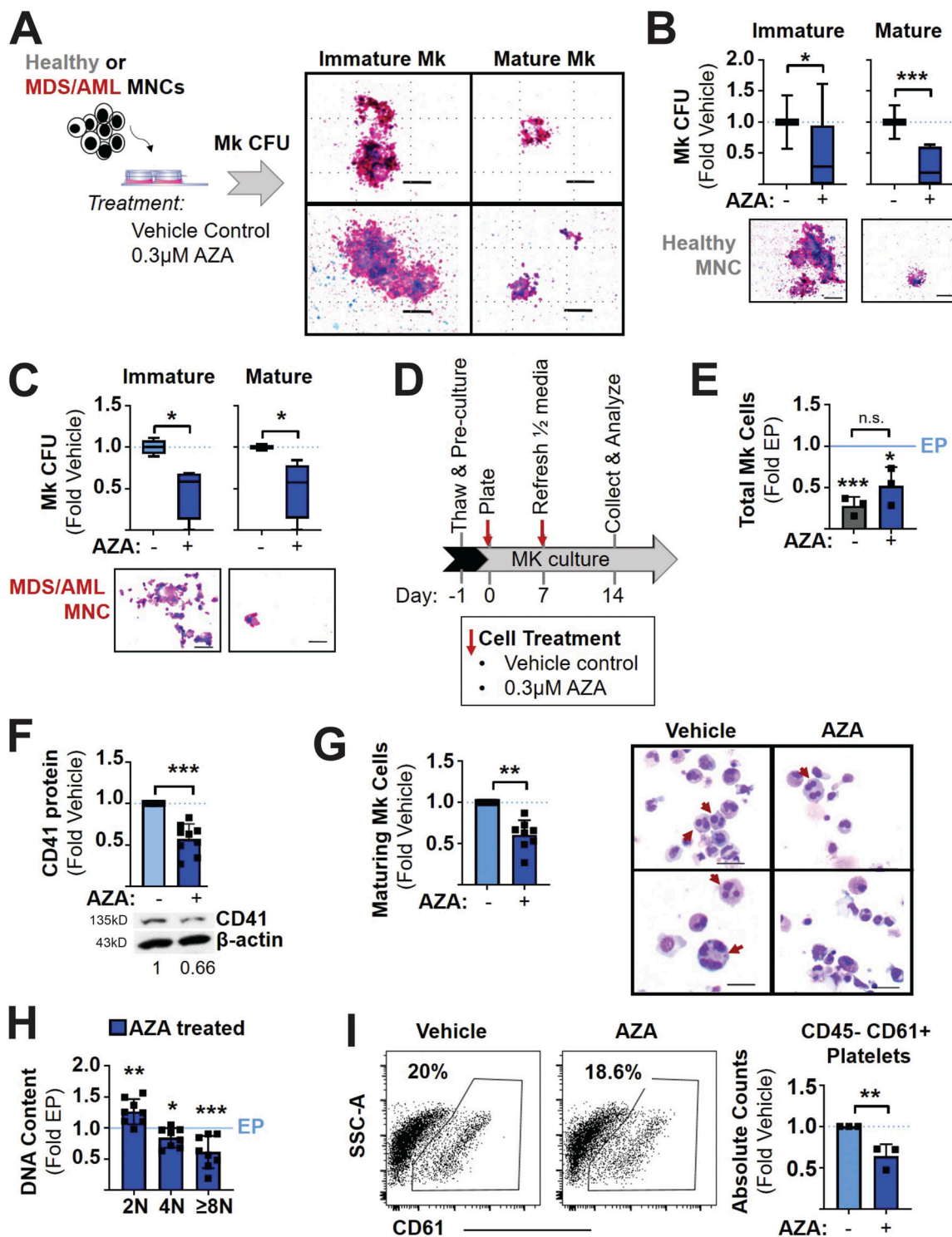
**Figure 1. AZA inhibits Mk progenitor growth and differentiation. (A–C)** Quantification of Mk CFU in primary MNC specimen by MegaCult assay (containing 0.5 µg/ml EP to stimulate Mk CFU growth) in the absence or presence of AZA (0.3 µM). **(A)** Experimental outline and examples of scored immature and mature Mk CFU picture inserts (scale bars indicate 100 µm). **(B and C)** Number of Mk CFU represented as box plots with min to max (whiskers) normalized to cultures lacking AZA (only containing EP) for healthy control-derived MNC (B; $N = 5$ biological specimens in independent experiments), and MDS/AML patient MNC (C; $N = 3$ independent biological specimens in independent experiments). Representative images of immature and mature Mk colonies are displayed below each subpanel (scale bar depicts 100 µm). **(D–H)** Assessment of Mk cell growth and differentiation in Mk promoting liquid cultures in the absence or presence of AZA. **(D)** Experimental outline. **(E)** The total number of CD41+ cMPL+ cells inferred from the total number of viable cells counted by Trypan Blue staining multiplied by the relative frequency of CD41+ cMPL+ cells (by FACS) on day 13 of the culture. Bar graphs depict averages ± SD for each group along with individual data points (filled squares) as fold changes normalized to Mk differentiation stimulated with EP but lacking AZA. $N = 3$ independent biological specimens. **(F)** Quantification of CD41 Mk protein following treatment of CB CD34+ in Mk differentiation cultures for 14 d by Western blot. Bar graphs represent mean CD41 protein ± SD quantified as fold change vehicle treated. $N = 4$ independent biological samples with technical repeats.

**(G)** Cytomorphological assessment of maturing Mk cells (left; red arrows; scale bar depicts 30 µm). Bar graphs (right) represent means of maturing Mk cells ± SD normalized to Mk differentiation–promoting cultures lacking AZA. N = 3 independent biological samples. **(H)** Polyploidy quantification by propodium iodide (PI) and CD41 co-staining, followed by FACS analysis. CD41$^+$ cells were sub-gated at 2N, 4N, or ≥8N for DNA content respectively. Bar graphs represent mean ± SD of frequencies of cells in each gate and expressed as fold changes compared with base cultures lacking Mk stimulation (by EP) and AZA (no treatment [NT] indicated by gray line); filled squares show normalized individual data values. N = 5 biological specimens in independent experiments. **(I)** Frequency of PLTs (CD45$^-$ CD61$^+$) cells. Absolute counts determined by CD45$^-$ CD61$^+$ FACS staining, manual counting, and count beads, and expressed as a fold change of vehicle control. Representative FACS plots (right). Bar graphs (left) depict mean PLT counts ± SD for three biological samples in independent experiments. Statistical significance indicated as *P < 0.05, **P < 0.01, ***P < 0.001 by Student's t test. Source data are available for this figure: SourceData F1.

returned to baseline by 4 d after treatment (Fig. S2 K). AZA rapidly elicited activation of the IFN-I response hallmarked by IFNα secretion (Fig. S2 L) and increased IFNβ levels within only 1 h of AZA (Fig. 3 J) or DEC (Fig. S2 M) treatment of MNC. Notably, purified CD34$^+$ cMPL$^+$ stem and progenitor cell populations harboring extensive Mk colony forming capacity showed the strongest increase of IFNβ-expressing cells upon AZA exposure compared with CD34$^-$ cMPL$^+$ MNC, which also harbors the lowest capacity for Mk cell generation (Fig. 3, K and L). To impair IFNβ production downstream of TLR3 activation, we chose BX795 (Clark et al., 2009), a chemical inhibitor of TANK-binding Kinase I and inhibitor of nuclear factor kappa B kinase subunit epsilon (TBK1/IKKε) and key mediator of TLR3 triggered IFN-I release (Fitzgerald et al., 2003), which resulted in a partial, statistically non-significant rescue (P = 0.055) of MDS/AML patient–derived Mk progenitor cells in AZA containing colony assays (Fig. 3 M).

Reactivation of endogenous retroviral (ERV) elements upon DNA demethylation can trigger viral mimicry within several days of HMA exposure (Chiappinelli et al., 2015; Li et al., 2014; Roulois et al., 2015; Stone et al., 2017). We probed whether the AZA-induced rapid IFN production coincided with ERV reactivation and DNA demethylation following short-term AZA treatment of MNCs and found no evidence for a robust reactivation of these immunogenic sequences upon acute exposure to AZA (Fig. S2, N–R). In line, assessment of DNA 5mC levels showed no changes at this early time point, albeit significant global DNA demethylation was detectable after 4 d of AZA treatment (Fig. S2 S), consistent with previous studies (Cheng et al., 2018). These data strongly suggest that AZA elicits a rapid activation of IFN production following the accumulation of hypomethylated immunogenic RNA species in MNC cells, including stem and Mk progenitor cells. This response appears to precede detectable global DNA hypomethylation and ERV reactivation, albeit the experimental strategy chosen does not exclude functionally relevant changes in DNA cytosine methylation at specific loci.

### Activation of IFNα/β receptor (IFNAR) signaling in megakaryocytes upon AZA treatment

We next tested whether cells with Mk potential would be able to elicit an IFN-I response upon binding of IFN-I cytokines to the IFNAR (Fig. 4 A). IFNAR is a heteromeric cell surface receptor composed of two subunits, IFNα/β R1 and IFNα R2 (Abramovich et al., 1994; Colamonici et al., 1994). Assessment of cell surface expression of R1 and R2 on healthy MNC revealed similar R1-positive cell numbers but a larger fraction of R2 positive cells within TPO-R/cMPL expressing MNC compared with the pool of

total MNC (Fig. S3, A and B). Quantification of IFNAR expressing cells within stem and progenitor cell populations uncovered more IFNAR$^+$ cells within the CD34$^+$cMPL$^+$ cell population compared with CD34$^-$cMPL$^+$ cells (Fig. S3, C and D). We further found that a greater number of CD34$^+$cMPL$^+$ cells co-expressed both cytokine receptor subunits on their cell surface compared with CD34$^-$ cMPL$^+$ cells (Fig. 4, B and C). These results strongly suggested that a substantial fraction of Mk progenitors (Fig. 3 L) can activate IFNAR upon AZA exposure and suggests their increased sensitivity to activation of this innate immune signaling pathway.

IFNAR signaling activates receptor-associated protein tyrosine kinases Janus kinase 1 (JAK1) and tyrosine kinase 2 (TYK2), and these, in turn, phosphorylate cytoplasmic transcription factors signal transducers and activators of transcription (STAT) 1 and 2a (Bromberg et al., 1996; Li et al., 1997; Stark and Darnell, 2012). In line, we found a moderate but significant increase in STAT1 phosphorylation in CD34$^+$ cMPL$^+$ cells upon treatment with AZA (Fig. 4, D and E; and Fig. S3 E), as well as STAT1-mediated gene target expression activation in healthy (Fig. 4 F) and patient-derived MNC (Fig. 4, G and H). We also detected increased expression of STAT1 target suppressor of cytokine signaling 1 (SOCS1) at the mRNA (Fig. S3 F) and protein levels after AZA treatment (Fig. 4 I). Furthermore, compared with paired pre-treatment specimens, the expression of a cluster of various IFN-I–stimulated genes (ISG; Fig. S3 G) and SOCS1 (Fig. S3 H) was elevated in patients under longer-term AZA therapy. Together, these results demonstrate that AZA treatment can trigger a rapid and persistent activation of IFNAR downstream signaling in healthy and leukemic MNC, including at the stem and progenitor cell levels.

### AZA-mediated IFN-I–dependent attenuation of TPO-R stimulation

MPL-expressing cells expressing high levels of functional IFNAR (Fig. 4 C) may activate downstream signaling in response to IFN-I activation. As SOCS proteins are known to inhibit cytokine receptor signaling (Piganis et al., 2011) through interaction with associated intracellular Janus kinases (Endo et al., 1997), we predicted that AZA-mediated IFN-I/STAT1/SOCS1 induction inhibited TPO-R signaling. To test this, we assessed TPO-R signaling in healthy or MDS/AML-derived MNC in the presence and absence of AZA focusing on canonical signaling components of the TPO-R, which critically relies on the activation of JAK2 (illustrated in Fig. S4 A; Endo et al., 1997; Zhang et al., 2018). AZA exposure of MDS/AML patient–derived (Fig. 5, A–D) or healthy MNC (Fig. 5, E–L) prevented the increase in phosphorylation of STAT3/5, AKT, and ERK upon TPO-R stimulation (Fig. S4, B and

Okoye-Okafor et al.
Mitigating azacitidine-mediated thrombocytopenia

Journal of Experimental Medicine
https://doi.org/10.1084/jem.20212228

4 of 17
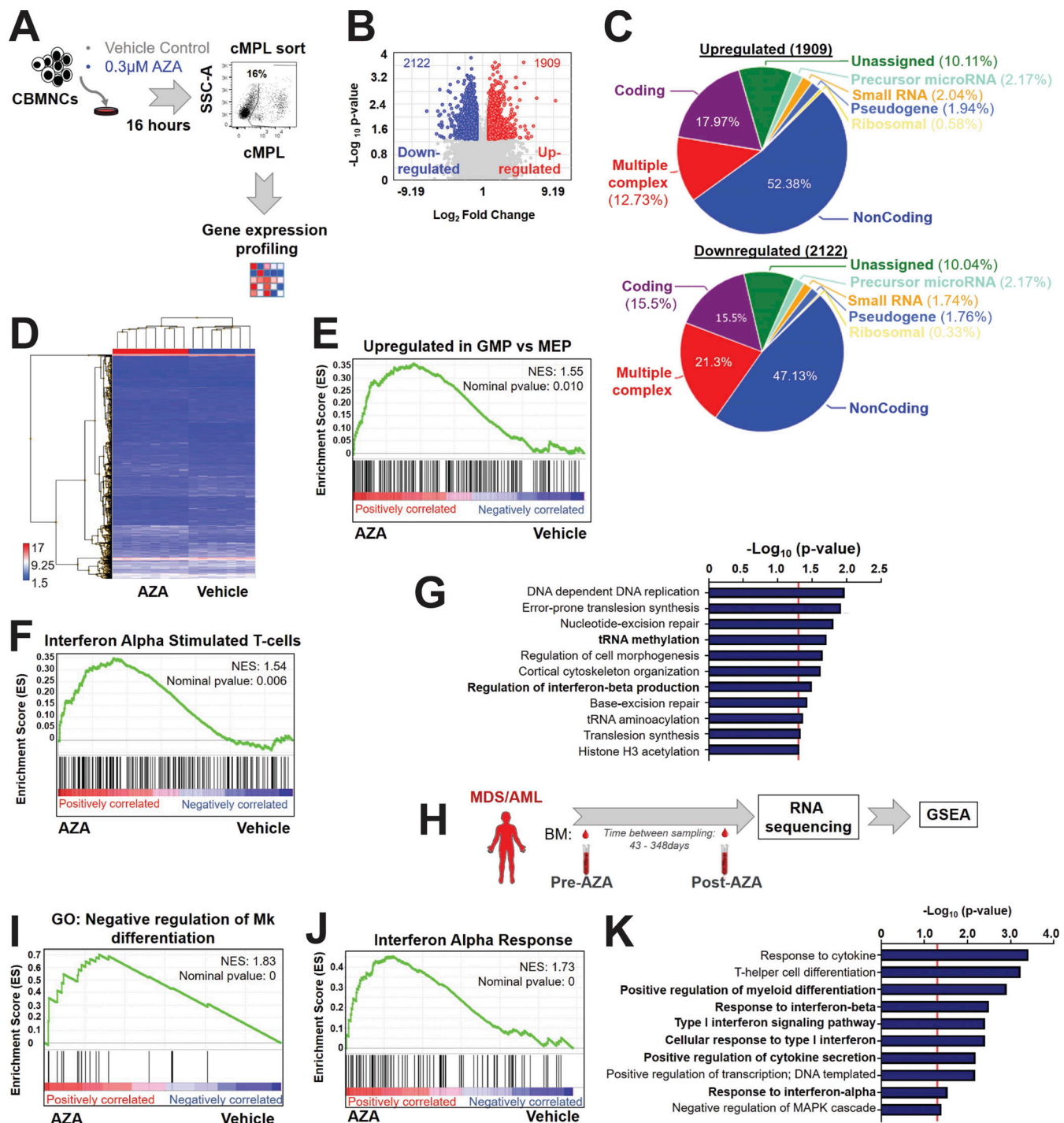
Figure 2. **AZA impairs Mk gene expression programs and induces IFN-I. (A–G)** Assessment of gene expression in FACS-sorted cMPL+ cells after culture of MNC for 16 h in TPO-R–stimulating conditions in the presence or absence of AZA. *N* = 3 biological samples in independent experiments. **(A)** Experiment outline. MNC were cultured in presence of TPO-RA (100 ng/ml hrTPO or 5 µg/ml EP) in the absence (vehicle control) or presence of AZA (0.3 µM AZA) before FACS sort for cMPL+ cells and subsequent microarray analysis. **(B)** Volcano plot depicting the distribution of differentially expressed genes in cMPL+ cells upon AZA treatment compared with vehicle-treated cells. **(C)** Assessment of genome-wide distribution of differentially expressed genes (upregulated genes, top pie chart; downregulated genes, bottom pie chart). **(D)** Hierarchical clustering analysis of differentially expressed genes. **(E and F)** GSEA identifies (E) significant upregulation of myeloid genes of granulocytic monocytic progenitors (GMP) versus Mk erythroid progenitors (MEP) in AZA-treated cells compared with vehicle control (GSE15330). **(F)** Significant enrichment of genes upregulated in IFNα-stimulated T cells after AZA treatment (normalized enrichment score = 1.54; nominal P value = 0.006; GSE40666). **(G)** IPA showing enrichment of biological processes upregulated in AZA-treated samples compared with controls (EnrichR analysis, GO Biological Process 2018). The red line represents the cutoff of significance (blue bars represent the –log$_{10}$ of the significance [P value]). **(H–J)** Differential gene expression by RNA-seq and GSEA enrichment analysis of differentially expressed genes in MDS/AML patient–derived MNC before and after AZA exposure in vivo. *N* = 7. **(H)** Experimental outline (Helsinki cohort). **(I)** GSEA enrichment of genes involved in negative regulation of Mk differentiation and upregulated after AZA treatment (normalized enrichment score = 1.83; nominal P value = 0; false discovery rate = 0.027). **(J)** Significant upregulation of

C; and Fig. 5, A–L). The addition of exogenous IFNα phenocopied this effect (Fig. S4, D–G). Conversely, pharmacological inhibition of IFNAR using dercernotinib, a highly specific JAK3 inhibitor (JAK3i; Farmer et al., 2015) previously shown to curtail AZA-triggered IFNAR activation (Roulois et al., 2015), or an IFNα/β-blocking B18R peptide (Alcami et al., 2000; Symons et al., 1995) led to a significant increase and restoration of pSTAT3/5, pAKT, and pERK levels in AZA-exposed Mk cells upon TPO-R stimulation using TPO (Fig. 5, E–H); while, except for pERK, no statistically significant alterations were seen with EP (Fig. 5, I–L). We conclude that AZA-mediated IFNAR activation can attenuate the stimulation of TPO-R signaling.

### Mitigating AZA-induced IFN-I signaling allows for efficient stimulation of megakaryopoiesis

To test whether the inhibitory effects of AZA on megakaryopoiesis were attributable to IFNAR activation, we quantified Mk progenitor cell frequencies in healthy or MDS/AML MNC specimens by colony assay in the presence of AZA alone or in combination with IFN-I inhibitors. We found that pharmacologic inhibition of IFN-I signaling normalized immature as well as mature Mk colony-initiating cell numbers in AZA-exposed healthy (Fig. 6 A and Fig. S5 A) and patient-derived cell cultures (Fig. 6 B). IFN-I signaling inhibition also led to a reversal of increased SOCS1 mRNA (Fig. 6 C) and protein levels (Fig. 6, D and E) after AZA treatment. Notably, SOCS1 expression returned to baseline levels by day four after AZA exposure (Fig. S5, B and C).

We next tested whether the return of SOCS1 to low baseline levels after treatment with AZA allowed for effective TPO-R mediated stimulation of megakaryopoiesis, for which we quantified stem and progenitor cell proliferation and differentiation in megakaryopoiesis stimulating cultures upon sequential treatment with AZA followed by TPO-RA (Fig. 6 F). This revealed the restoration of immature and mature Mk colony-forming cell numbers in sequentially treated cultures compared with cell cultures simultaneously exposed to AZA and TPO-RA (Fig. 6 G). The sequential treatment regimen also increased the number of CD41 expressing cells by 30% (Fig. 6 H and Fig. S5 D) compared with cultures simultaneously exposed to AZA and the TPO-RA. Moreover, RNAi-mediated down-regulation of SOCS1 (Fig. S5 E) rescued AZA-mediated inhibition of STAT5 activation (Fig. S5 F).

Lastly, IFN-I signaling is critical in the context of anti-leukemic therapies (Benjamin et al., 2007). Therefore, curtailing its activation through the use of direct IFN signaling inhibitors may blunt crucial immune-mediated leukemic cell eradication pathways. To circumvent this potential caveat, we focused on P38 mitogen-activated protein kinase (p38 MAPK, p38) which is involved in the execution of IFNα-mediated anti-viral responses (Bachegowda et al., 2016; Mayer et al., 2001). We

found higher levels of phosphorylated p38 in AZA-treated cells compared with controls (Fig. 6 I) and observed that pharmacological inhibition of p38 counteracted the inhibitory effects of AZA on megakaryocyte progenitor growth stimulation (Fig. 6 J). Taken together, these results support that mitigating the activation of IFN-I signaling via the use of p38 inhibitors which have been tested for therapy of MDS (Bachegowda et al., 2016; Garcia-Manero et al., 2015) may allow for effective enhancement of Mk progenitor cell growth and differentiation in patients with MDS/AML undergoing therapy with AZA.

## Discussion

Our observations of AZA-induced innate immune signaling in MNC and its inhibitory effects on megakaryopoiesis (Fig. S5 G) are in line with well-documented anti-Mk/anti-thrombocytic effects of IFNα (Haas et al., 2015; Wang et al., 2000), particularly in patients with essential thrombocytosis (Mazur et al., 1986). We found that increased IFN-I dependent gene expression in MNC from longitudinally monitored patients is consistent with past reports on AZA and DEC-mediated activation of IFN-I response following DNA hypomethylation, the reactivation of ERV sequences upon long-term exposure (Chiappinelli et al., 2015; Roulois et al., 2015).

Moreover, our study uncovered a novel mode of IFN-I signaling activation in several MNC populations which appears to precede datable global DNA hypomethylation and ERV reactivation; we also found it to be acute and transient. In line with previous studies reporting AZA-mediated inhibition of RNA methylation, particularly affecting tRNAs (Schaefer et al., 2009; Schaefer et al., 2010), we detected rapid RNA cytosine demethylation in concert with dsRNA accumulation and activation of IFN-I anti-viral signaling upon AZA in MNC and purified MPL[+] stem and progenitor cells. Our data strongly suggest that DEC elicits a very similar response. Thus, acute RNA demethylation upon AZA treatment is unlikely to stem from direct RNA intercalation, but rather a consequence of an upstream event, e.g., alterations in methyl group metabolism. Whether HMA and other anti-leukemic regimens eliciting thrombocytopenia share a molecular mode of action remains to be determined.

The observed functional impairment of specifically Mk progenitor cell expansion and differentiation after AZA exposure occurs in both healthy control and MDS/AML patient–derived primary MNC supports that AZA affects patient-derived stem and progenitors capable of Mk lineage differentiation. To unequivocally test this prediction, differential effects of AZA on healthy residual, preleukemic, and leukemic cell clone growth and their respective Mk lineage potential will need to be assessed. Albeit, we found rapid IFN-I signaling induction in various MNC subpopulations, and its impact at the functional level appears to be cell context-specific (exerting inhibitory
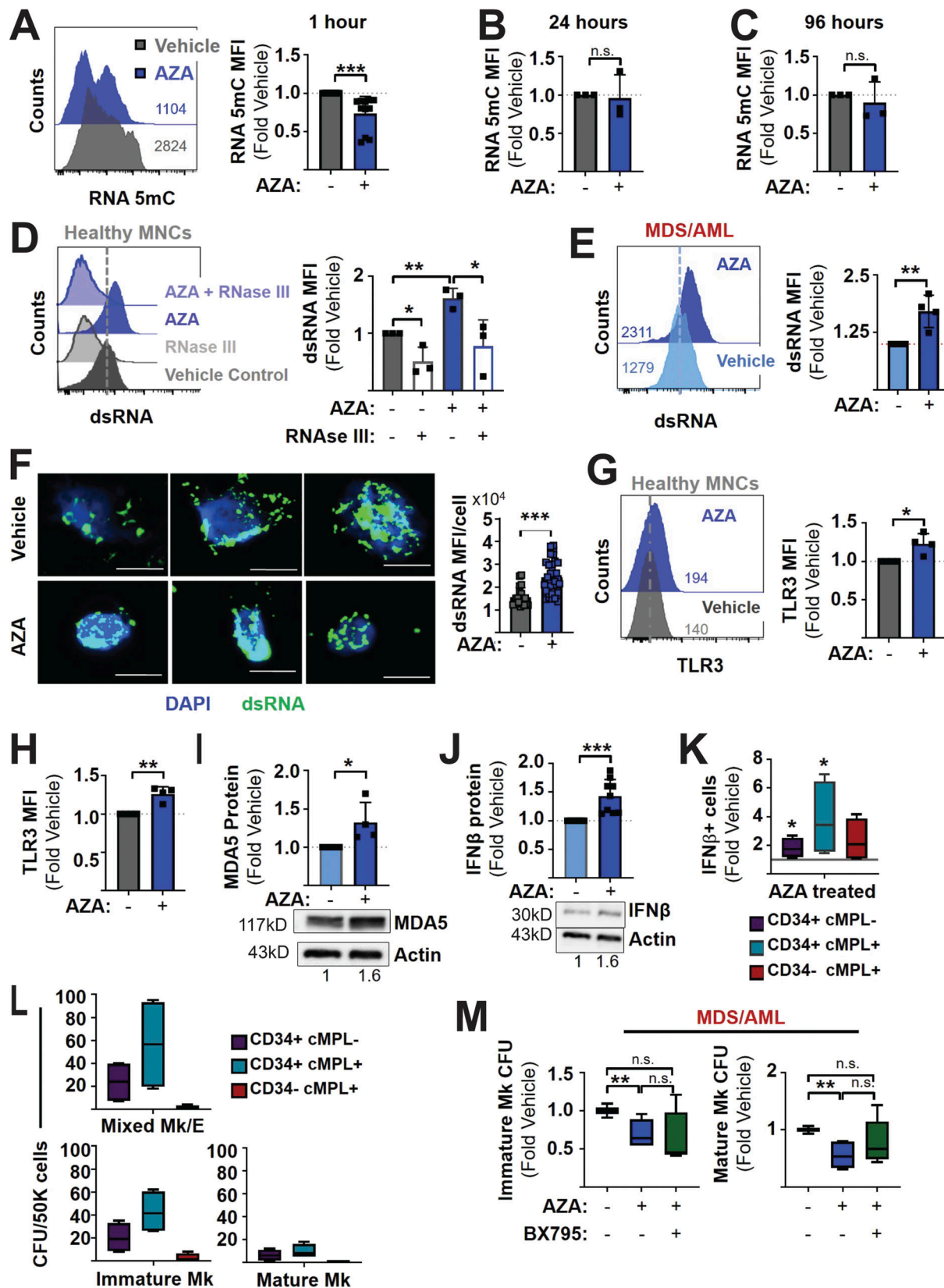
Figure 3. **Innate immune pathway activation upon AZA in MNC and Mk cell populations. (A–C)** Quantification of RNA 5-methyl cytosines (RNA 5mC) by FACS analysis of CB-MNC in the absence or presence of AZA (0.3 µM) in Mk-promoting cultures. Bar graphs represent quantifications of RNA 5mC normalized mean fluorescence intensity (MFI) at each time point as mean ± SD along with individual data points (filled squares; $N$ = 3–11 independent experiments and biological replicates). **(A)** Representative FACS histogram (left; control [gray] and AZA [blue]; counts normalized to modal) and quantification of MFI (right)

normalized to controls devoid of AZA at 1 h, 24 h (B), and day 4 (C). **(D–F)** Quantification of dsRNA in cells after a 1 h Mk-promoting culture in the absence or presence of AZA. **(D and E)** dsRNA quantification in MNC by FACS analysis. RNAseIII-treated cells as background controls. Representative histogram depicts counts normalized to modal. Bar graphs represent changes in dsRNA expressed as fold changes of control (mean) ± SD of CB or BM-MNC ($N$ = 3 biological samples in independent experiments; D), and MDS/AML patient–derived MNC ($N$ = 4 biological samples in independent experiments; E). **(F)** Immunocyto-chemistry and confocal fluorescence microscopy to visualize dsRNA (green) along with nuclear staining (DAPI/blue) in CB-derived CD34$^+$ cells in cultures lacking AZA (vehicle [–]) or upon exposure to AZA (0.3 µM; left representative images of cells; scale bar: 10 µm). Bar graphs show significantly increased dsRNA species in the presence of AZA compared with vehicle-treated control cells. Bar graphs depict mean ± SD of MFI per cell for each group along with individual data points ($N$ = 2 biological specimens; 21–37 cells/field of view). **(G and H)** Quantification of TLR3 protein levels by flow cytometry after 1 h of culture in Mk-promoting medium in the absence (vehicle, –) or presence of AZA in healthy MNC (G), or CD34$^+$ cells (H). **(I)** MDA5 protein levels by Western blot analysis 24 h after treatment. Bar graphs represent mean MDA5 expression ± SD normalized to actin loading control. Representative blot displayed underneath. **(J)** IFNβ protein expression by Western blot within 24 h of treatment in absence or presence of AZA. Bar graphs represent mean protein ± SD normalized to actin loading control. Representative blot displayed underneath. $N$ = 4 independent biological specimens in technical duplicates. **(K)** Assessment of intracellular IFNβ levels by flow cytometry after 1 h of culture in the absence (vehicle) or presence of AZA in Mk progenitor cell populations. Quantification of the fraction of IFNβ$^+$ cells within each cell population. Graph shows relative cell frequencies of IFNβ$^+$ cells normalized to vehicle controls represented as box plots with min to max (whiskers); $N$ = 3 independent biological specimens in independent experiments. **(L)** Quantification of Mk CFU within purified CD34$^+$ cMPL$^-$ immature myeloid, CD34$^+$cMPL$^+$ Mk progenitor, and CD34$^-$ cMPL$^+$ mature Mk cell populations by MegaCult assay. $N$ = 3 independent experiments and biological samples. **(M)** Quantification of MDS/AML MNC-derived Mk CFU in the presence of AZA and upon TLR3 downstream signaling inhibition by TBK1/IKKe inhibition (BX795) in MegaCult assays. Box plots show the number of immature Mk (left) and mature Mk (right) CFU and min to max (whiskers) normalized to TPO only cultures. $N$ = 4 biological replicates in independent experiments. Statistical significance indicated as *P < 0.05, **P < 0.01, ***P < 0.001 by Student's $t$ test; n.s., not significant. Source data are available for this figure: SourceData F3.

effects in Mk-potent, but not other myeloid progenitor cells). We attributed this effect to premature TPO-R signaling attenuation, which was observed following AZA exposure of MNC stimulated with endogenous TPO or EP. Pharmacologic mitigation of IFN-I signaling activation restored TPO-R signaling in cells stimulated with TPO, but to a lesser extent in cells treated with EP. This finding may stem from the differences in eliciting cMPL downstream signaling due to differences in binding the receptor (TPO binds the extracellular ligand binding domain triggering strong STAT5/3 and MAPK activation; while EP binds the jux-tamembrane domain eliciting strong STAT5 and delayed STAT3 and slightly differential MAPK activation; Erickson-Miller et al., 2009; Will et al., 2009).

Contrary to its inhibitory effects in Mk lineage-committed progenitor cells, IFN-I can activate quiescent stem cells and increase Mk lineage output (Essers et al., 2009; Haas et al., 2015). It is tempting to speculate that AZA/IFN-I triggers the expansion of non-leukemic cells, and Mk differentiation competent HSPC may compensate for the inhibitory effects of AZA/IFN-I on lineage committed Mk progenitor cells, thus alleviating inef-fective megakaryopoiesis seen during early phases of AZA therapy. Further studies into the dynamics of leukemic and re-sidual healthy stem cell generation and differentiation under AZA therapy need to be carried out to clarify this relevant aspect.

Lastly, our data show that mitigation of AZA-mediated in-hibitory effects on megakaryopoiesis is possible via inhibition of IFN-I activation. Activated by IFN-I signaling, p38 MAPK acti-vation is among myelosuppressive signals in human hema-topoiesis; inhibition of this pathway showed pre-clinical (Bachegowda et al., 2016) and clinical efficacy (Garcia-Manero et al., 2015) in the management of MDS/AML improving ery-throid and myeloid blood cell generation. Our data demon-strate that low-dose p38 inhibitor treatment can restore megakaryopoiesis and strongly suggests that clinically avail-able p38 inhibitors, such as ARRY-614 (Garcia-Manero et al., 2015), may offer a suitable strategy to alleviate AZA-mediated thrombocytopenia.

## Materials and methods

### Study design
The purpose of the study was to define the molecular and functional consequences of AZA treatment on megakaryopoiesis. Mk differentiation potential of primary hematopoietic cells de-rived from human cord blood (CB), peripheral blood (PB), or BM was analyzed in the absence or presence of AZA. IFN-I–signaling induction was rescued using JAK3 inhibitor dercernotinib (VX509), IFNα-blocking peptide B18R, genetic inhibition of SOCS1, or inhibitors of TBK1 (BX795) or p38 (SB203580).

### Reagents
#### EP
EP (provided by Novartis) was dissolved in ddH$_2$O at 10 mg/ml. Working stock dilutions of 0.5 or 0.3 mg/ml EP were prepared and filtered.

#### AZA
AZA (cat. #A72012; Sigma-Aldrich) was reconstituted in 1× diluted Dulbecco's PBS (cat. #14200075; Thermo Fisher Scientific) at 40 mM and stored at –20°C in single-use aliquots. DEC (cat. #A3656; Sigma-Aldrich) was reconstituted in DMSO (cat. #D128-500; Fisher Chem-ical) at 50 mg/ml and stored at –20°C in single-use aliquots.

#### Recombinant human cytokines
Recombinant human cytokines were all purchased from Gemini. IFNα (rhIFNα; cat. #300-206P), stem cell factor (rhSCF; cat. #300-07), TPO (rhTPO; cat. #300-188P), IL-3 (rhIL3; cat. #AF-200-03), and IL-6 (rhIL-6; cat. #AF-200-06) were reconstituted and stored according to the manufacturer's recommendation. Recombinant vaccinia virus B18R protein (cat. #ab190383) was reconstituted at 0.2 mg/ml and stored in single-use aliquots at –80°C.

#### Decernotinib
Decernotinib (cat. #S7541; Selleckchem) was reconstituted at a concentration of 50 mM in DMSO (cat. #BP231-100; Thermo Fisher Scientific). Stocks were stored as single-use aliquots at –20°C.
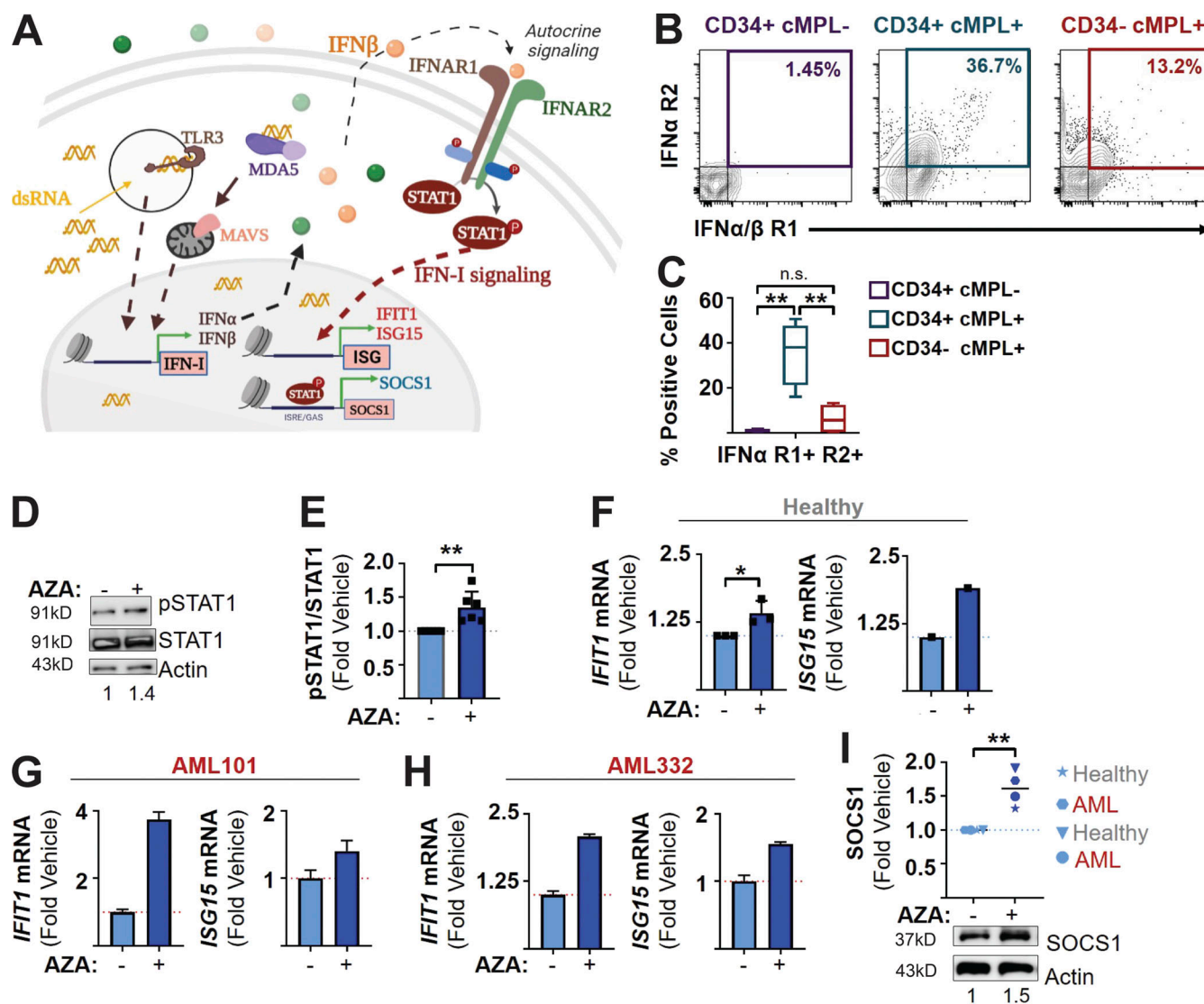
Okoye-Okafor et al.
Mitigating azacitidine-mediated thrombocytopenia

Journal of Experimental Medicine
https://doi.org/10.1084/jem.20212228

8 of 17

**Figure 4.** **Activation of IFNAR signaling upon AZA exposure. (A)** Mechanistic scheme on autocrine IFNAR receptor activation. **(B and C)** Quantification of IFNAR1 and IFNAR2 cell surface proteins on CD34+ cMPL−, CD34+ cMPL+, and CD34− cMPL+ cells by FACS. Representative FACS plots for IFNα/β R1 IFNα/β R2 expression in parental cell populations (indicated on top of plots; B) and (C) quantification of relative frequencies of cells expressing responsive heterodimeric IFNAR receptors (IFNα/β R1+ IFNα/β R2+ cells) within parental cell populations represented as box plots with min to max (whiskers); N = 4 biological specimens in independent experiments. **(D and E)** Quantification of phosphorylated (pSTAT1) and total STAT1 protein levels by Western blot analysis upon AZA treatment of CB MNCs for 1 h in Mk-promoting cultures (containing 5 μg/ml EP) in the absence or presence of AZA (0.3 μM). Example blot (D) and bar graphs representing mean pSTAT1 protein levels ± SD normalized to total STAT1 protein and actin loading controls (E). N = 3 independent biological specimens in technical duplicates. **(F–H)** Quantification of STAT1/IFN-I target expression, *IFIT1* (left), and *ISG15* (right) by qRT-PCR analysis in cells after Mk prompting culture (containing 5 μg/ml EP) in the absence (control) or presence of AZA. Bar graphs represent *GAPDH*-normalized average expression values ± SD depicted as fold changes to control cultures as well as individual data points in healthy MNC after culture for 2 h (F), and AML patient–derived MNC after culture for 2 h (G), as well as 24 h (H). **(I)** SOCS1 protein expression by Western blot analysis in healthy or AML MNC after 1 h culture in the absence or presence of 0.3 μM AZA. Black line represents mean expression of actin-normalized individual protein levels depicted as fold changes to vehicle control. N = 2 (healthy) and 2 (AML) in independent experiments. Statistical significance indicated as *P < 0.05, **P < 0.01, ***P < 0.001 by Student's *t* test (C, E, F, and I); n.s., not significant. Source data are available for this figure: SourceData F4.

### SB 203580

SB 203580 (cat. #559398; Millipore Sigma) was stored as single-use aliquots at −20°C. Prior to use, the stock was pre-diluted with medium to 500 μM and used immediately.

### BX795

BX795 (cat. #S1274; Selleckchem) was resuspended in DMSO at a concentration of 10 mM and stored as single-use aliquots at

−80°C. Before use, stocks were diluted with medium to a working stock concentration of 100 μM (100×) and used immediately.

### Primary cells

Human BM or PB specimens were collected at Montefiore Medical Center and the Albert Einstein College of Medicine (Table S1). Work conducted by this observational study was

Okoye-Okafor et al.
Mitigating azacitidine-mediated thrombocytopenia

Journal of Experimental Medicine    9 of 17
https://doi.org/10.1084/jem.20212228
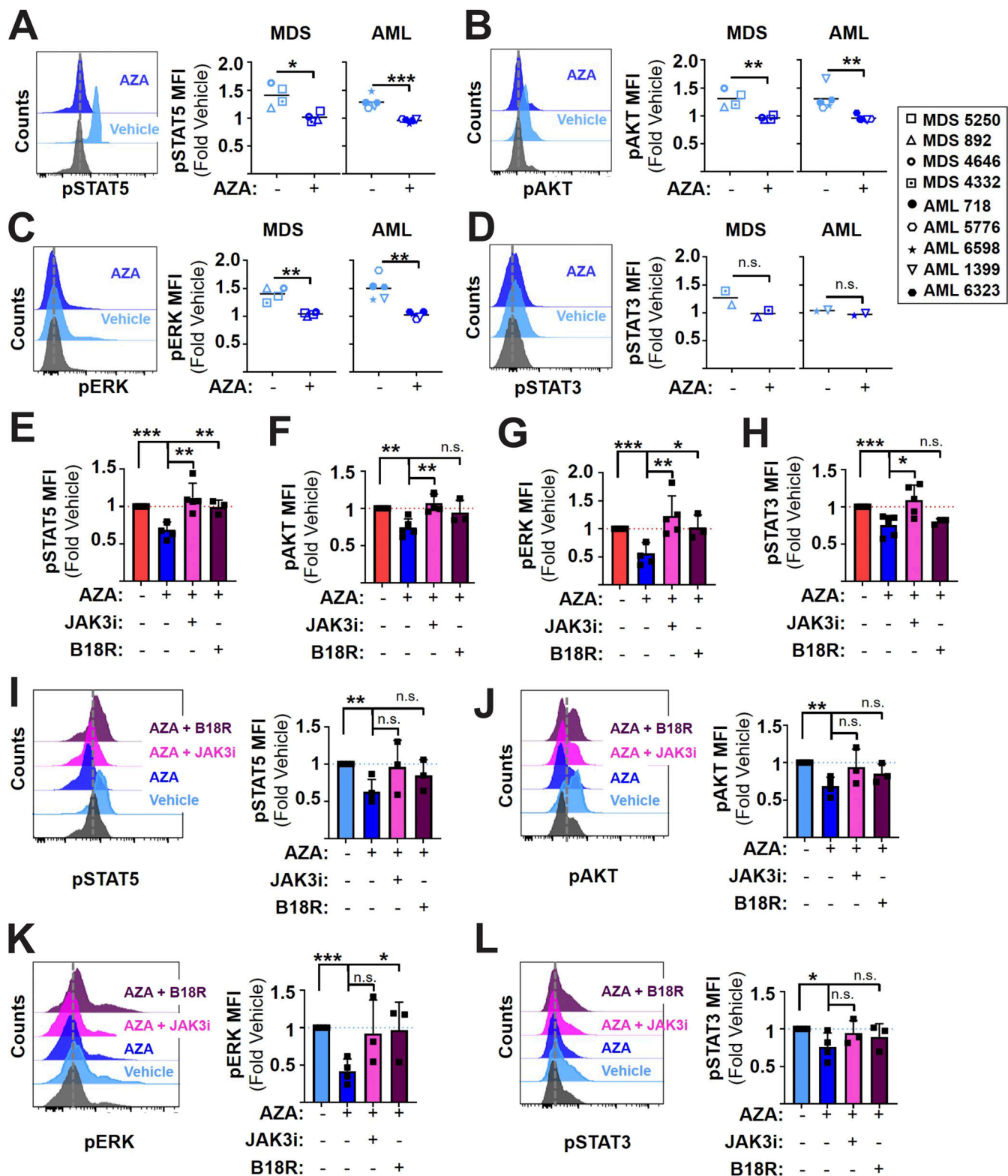
**Figure 5. AZA impairs stimulation of TPO-R signaling in an IFN–I–dependent manner. (A–D)** Quantification of TPO-R downstream signaling by phosphoflow analysis in MDS and AML patient BM-derived NC upon a 1 h culture to stimulate TPO-R (with 1 µg/ml EP) in the absence (vehicle) or presence of AZA (0.3 µM); cells in cultures lacking TPO-R stimulation as base line (gray). pSTAT5 (A), pAKT (B), pERK (C), and pSTAT3 (D) were measured on viable, single CD45 expressing cells. Representative histograms (left) show counts normalized to modal from healthy donor MNC. Graphs (right) depict mean MFI levels as fold change of baseline (no TPO-R) controls ± SD; $N$ = 2–4 biological samples in independent experiments. **(E–H)** TPO-R downstream signaling in CB MNC stimulated with 100 ng/ml TPO, in the absence or presence of 0.3 µM AZA, or in combination with either VX-509 (JAK3i; 0.3 µM) or B18R peptide (1 µg/ml). Bar graphs depict mean MFI ± SD of pSTAT5 (E), pAKT (F), pERK (G), and pSTAT3 (H) in CD34+ cMPL+ immature Mk cells normalized to vehicle control. **(I–L)** Analysis of TPO-R stimulation (by EP) in healthy MNC treated for 1 h in the presence or absence of 10 ng/ml rhIFNα. Followed by evaluation of pSTAT5 (I), pAKT

(J), pERK (K), and pSTAT3 (L) by phosphoflow analysis. Representative histogram plots depicting counts normalized to modal are shown. Bar graphs depict means ± SD of MFI values normalized to EP or TPO continuing control cultures lacking AZA; $N = 3$ independent experiments and biologic specimens. Statistical significance indicated as *$P < 0.05$, **$P < 0.01$, ***$P < 0.001$ by Student's $t$ test; n.s., not significant.

approved by the Albert Einstein College of Medicine's Institutional Review Board (#2016-6770). Healthy control BM and CB specimens were purchased from Lonza and the New York Blood Bank, respectively. MDS/AML patient samples were longitudinally collected before and after AZA treatment using a protocol approved by an ethics committee at Helsinki University Hospital (303/13/03/01/2011) and were processed at Institute for Molecular Medicine Finland (FIMM; Helsinki, Finland; Table S5). Cells were maintained in recovery cultures in StemSpan SFEM (cat. #09650; StemCell Technologies) supplemented with 50 ng/rhSCF and 100 µg/ml Primocin (cat. #ANTPM1; Invivogen) at 37°C in 5% $CO_2$ in a fully humidified atmosphere for up to 24 h before use. All treatments were performed in cultures containing cells at a density of $0.5 – 1 \times 10^6$/ml. Please note that because of considerable baseline inter-sample variability, we resorted to the statistical analysis of mock-control normalized data for the specimen tested. To ensure data robustness, we have used biological repeats (as opposed to technical repeats), which result in data representations without variances in the controls.

### MNCs
MNCs were isolated using low-density Ficoll-Paque Plus (1.077 g/ml, cat. #17-0300; GE Healthcare Life Sciences) gradient centrifugation at 400 $g$ for 30 min at room temperature (RT). Before gradient centrifugation, PB and CB specimens were depleted of red blood cells for 30 min at RT using 5% (w/v) dextran (MW 266000; Sigma-Aldrich) in 0.9% $NaCl_2$.

### CD34+ HSPCs
CD34+ HSPCs were enriched from MNC by immunomagnetic bead sorting using the CD34 MicroBead Kit, human (cat. #130-046-702; Miltenyi Biotec) according to the manufacturer's protocol.

### Cell cultures
#### UKE-1 cell culture
UKE1 cells were grown in RPMI 1640 with glutamine (Corning) supplemented with 5% FBS (cat. #900-208; Gemini BioProducts), 1% penicillin/streptomycin (cat. #30-002-Cl; Corning), 1% HEPES buffer (cat. #25-060-CI; Corning), 1 µM hydrocortisone (cat. #H4001-1G; Sigma-Aldrich) at 37°C in 5% $CO_2$ in a fully humidified atmosphere. UKE1 cells were assured to be free of *Mycoplasma* contaminations.

#### TPO-R stimulation cultures
MNC were grown in StemSpan SFEM supplemented with TPO-RA (rhTPO or EP, at concentrations as indicated) and 100 µg/ml Primocin at 37°C in 5% $CO_2$ in a fully humidified atmosphere for 1–24 h, as indicated.

#### Quantification of ex vivo Mk differentiation and PLT production
CD34+ cells were grown in StemSpan SFEM supplemented with 5 ng/ml rhIL3, 50 ng/ml rhSCF, 20 ng/ml rhTPO, 20 ng/ml

rhIL-6, and 100 µg/ml Primocin at 37°C in 5% $CO_2$ in a fully humidified atmosphere for a total of 14 d. The culture medium was refreshed every 2–3 d; treatments were refreshed after 7 d of culture.

#### MegaCult assay to enumerate Mk progenitor cells
Assay setup, cell culture, and colony scoring were performed according to the manufacturer's protocol (cat. #04961; StemCell Technologies). Fixed and stained colony assays were imaged using a Cytation 5 inverted microscope (Bio-Tek) or an EVOS FL Auto (Thermo Fisher Scientific) in scanning mode. Colony morphology was assessed, and colony numbers were enumerated manually. Assays containing at least 10 clearly visible and identifiable Mk CFU were used for data analysis.

#### Sequential treatment cultures
For the first 4 d, CD34+ cells were subjected to liquid cultures at a density of $8 \times 10^4$ cells/ml at 37°C in 5% $CO_2$ in a fully humidified atmosphere in Mk differentiation cultures supplemented with either 5 µg/ml EP (group A; EP) or 5 µg/ml EP and 0.3 µM AZA (group B; EP + AZA) or 0.3 µM AZA (group C). After this initial liquid culture phase, half of the cells were continued in liquid cultures with refreshed medium and treatment supplements for an additional 10 days, and the other half was subjected to Mk progenitor enumeration in MegaCult assays. To group C culture (liquid and MegaCult), EP (5 µg/ml) was also added (AZA → D4 EP).

### Characterization of megakaryopoiesis
#### Morphologic analysis
Cells were cytospun upon culture completion. Cytospins were prepared using a Cytofuge (Statspin). Cell morphology was examined after May-Grünwald Giemsa staining (Cat. #660; Millipore Sigma) and documented using a Cytation 5 (BioTek) inverted microscope.

#### Cell surface marker analysis
Cells were stained with the following antibodies: anti–human cMPL PE (BD Pharmingen), anti–human CD34 PB (Biolegend), and anti–human CD41a fluorescein isothiocyanate (eBioscience). Details pertaining to the antibodies used are listed in Table S8.

#### Isolation of Mk cells for gene expression analysis
Upon a 16-h Mk differentiation culture in the presence or absence of AZA (0.3 µM), MNC were stained with anti-human cMPL PE (BD Pharmingen). Details pertaining to the antibodies used are described in Table S8. cMPL+ cells were sorted using a MoFlo ASTRIOS (BD Biosciences) cell sorter. Sorted cells were spun down at 300 $g$ at RT and lysed using RLT lysis buffer for RNA extraction and downstream analysis.
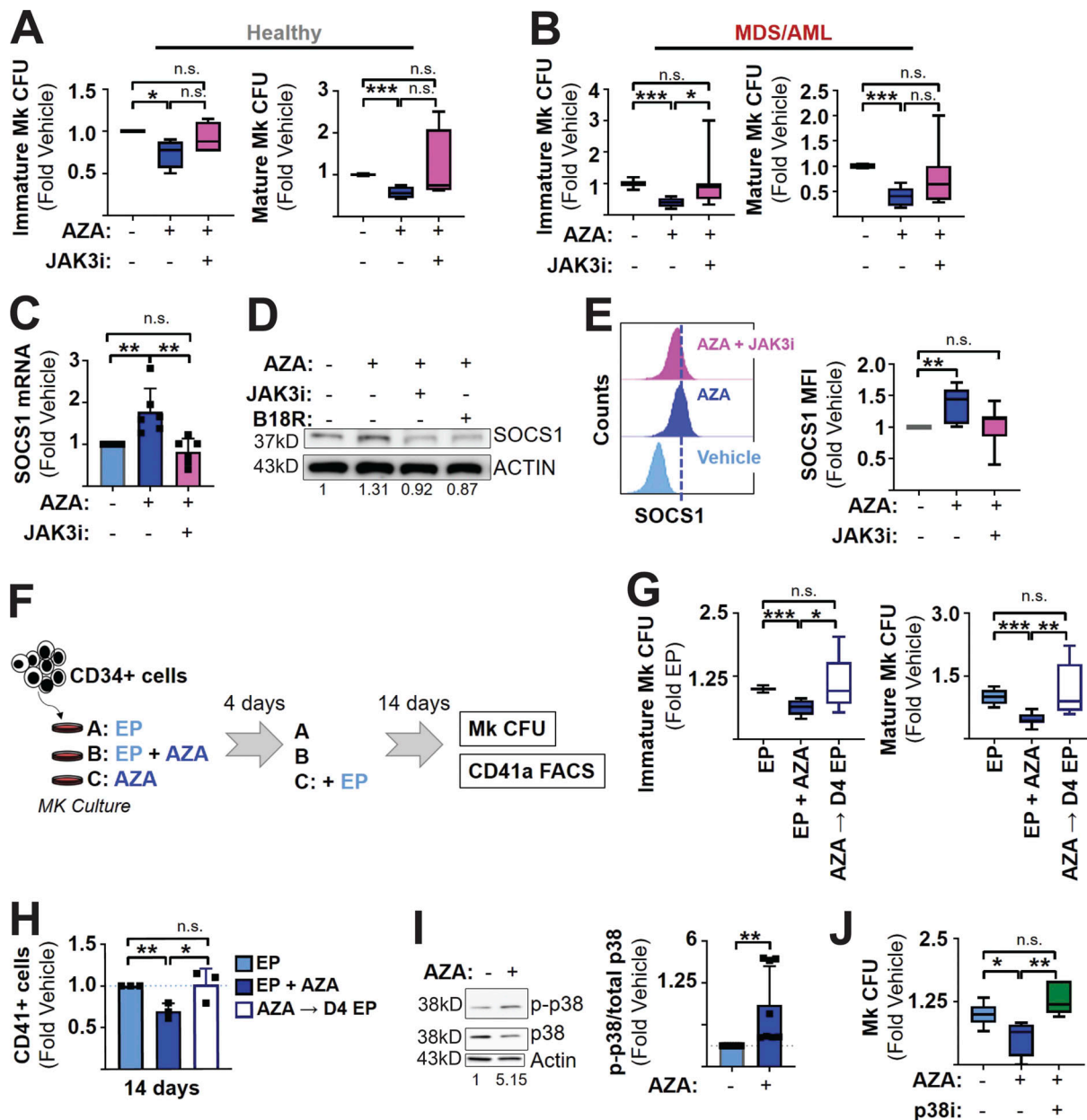
Okoye-Okafor et al.
Mitigating azacitidine-mediated thrombocytopenia

Journal of Experimental Medicine
https://doi.org/10.1084/jem.20212228

11 of 17

Figure 6. **Inhibition of IFN-I signaling restores megakaryopoiesis in the presence of AZA. (A and B)** Quantification of Mk CFU in MNC specimen by MegaCult assay (containing TPO-RA [100 ng/ml hrTPO or 5 µg/ml EP]) in the absence or presence of AZA (0.3 µM) alone or in combination with 0.3 µM JAK3i (VX-509). Box plots show the number of immature Mk (left) and mature Mk (right) CFU and min to max (whiskers) normalized to EP single agent control cultures. N = 9 biological replicates in independent experiments. Mk CFU quantification using healthy CB MNC specimen (A), or (B) MDS/AML patient–derived MNC (B). **(C–E)** Quantification of SOCS1 expression after TPO-R–stimulating culture (containing 100 ng/ml TPO or 5 µg/ml EP) in the absence or presence of AZA alone, or along with 0.3 µM VX-509 or 1 mg/ml B18R peptide. **(C)** Quantification of *SOCS1* mRNA by qRT-PCR after 2 h. Bar graphs represent *GAPDH* normalized relative mRNA expression means (arbitrary units) ± SD normalized to vehicle control. **(D and E)** SOCS1 protein quantification measured by (D) Western blot and (E) intracellular flow cytometry. Left: Representative FACS histogram depicting cell counts normalized to modal. Right: Box plots show the MFI values and min to max (whiskers) for SOCS1 protein expressed as fold changes vehicle control. N = 7 biological samples in independent experiments. **(F–H)** Sequential treatment with AZA rescues its inhibitory effects on Mk progenitor growth, differentiation, and maturation. **(F)** Experimental scheme outlining the sequential treatment culture model using CD34+ cells. **(G)** Number of Mk CFU represented as box plots with min to max (whiskers) enumeration by MegaCult assays in the presence of either EP alone throughout (EP; group A), EP and AZA throughout (EP+AZA; group B), or AZA in liquid pre-culture and subsequent addition of EP (AZA → D4 EP; group C) as fold changes compared with EP single agent cultures (group A); N = 3 biological replicates in four independent experiments. **(H)** FACS analysis of CD41 expressing cells after 14 d in sequential treatment liquid culture (as outlined in F). Bar graphs depict means of CD41-positive cell frequencies within viable singe cell parental populations normalized to EP single agent containing cultures ± SD for three independent experiments and biological samples. **(I)** Total p38, phospho-p38 (p-p38), and β-actin protein levels in healthy control or AML-derived MNC cultured in Mk-stimulating conditions (containing 5 µg/ml EP) in the absence or presence of AZA by Western blot (representative blot image [left] and automated image analysis assisted signal quantification [right]). Bar graphs represent β-actin normalized mean signal intensity (area under the curve) ± SEM of independent biological samples and experiments (N = 3). **(J)** Quantification of Mk CFU (MegaCult assays containing 5 µg/ml EP) of healthy control or AML patient–derived MNC cultured in the absence or presence of AZA with and without addition of 5 µM p38 inhibitor (p38i) SB203580. Box plots show the total number of Mk CFU and min to max

### Polyploidy analysis

Polyploidization was analyzed by propidium iodide (PI) and CD41a co-staining and cells were analyzed using an LSRII analyzer (BD Biosciences) as before with minor modifications.(Mattia et al., 2002) Details pertaining to the antibodies used are described in Table S8.

### FACS

Flow cytometry data were collected on a Special Order ARIA II or LSR II flow cytometer (both from BD Biosciences) using FACS-Diva software (BD Biosciences) or high throughput iQue Screener PLUS (Intellicyt). FACS data were analyzed using FlowJo software v10 (Treestar). All details for antibodies used in this study are listed in Table S8. Detailed procedures can be found in the supplemental methods section.

### Phosphoflow

Phosphorylation of the signal transducer and activator of transcription (STAT) 5 and 3 was determined after serum starvation in cytokine-free StemSpan SFEM for 1 h, as previously described (Karjalainen et al., 2017; Will et al., 2009). Cells were stained with Alexa 647-anti-phospho-Stat5 (pY694), PE-CF594-anti-phospho-Stat3 (pY705), BV421-anti-phospho-Akt (pS473), and PE-anti-phospho-Erk1/2 (pT202/pY204; all antibodies from BD Biosciences) using 1:10–1:20 dilutions.

### dsRNA detection

MNC or CD34+ cells were fixed with 3.7% paraformaldehyde for 15 min at RT, washed twice with 1× PBS at RT, and permeabilized with 0.2% T-PBS for 30 min at RT. The cells were washed twice in 1× PBS and the protein-bound nucleic acids were released by incubation of the permeabilized cells with proteinase K for 1 h at 37°C. Additionally, antibody specificity was tested using RNase III treatment for 1 h at 37°C. Cells were washed and stained with dsRNA-specific antibodies on ice for 30 min. Cells were washed twice with 1× PBS, stained with a rabbit anti-mouse AF488 secondary antibody (cat. #31584; 1:1,500; Life Technologies) for 30 min at RT, washed, and analyzed immediately.

### SOCS1 quantification

Cells were stained with anti-cMPL and anti-CD34 antibodies in culture for 15 min followed by immediate fixation with pre-warmed BD Cytofix buffer (BD Biosciences) for 12 min at 37°C. After washing, cells were permeabilized in cold BD Perm Buffer III for 30 min on ice, washed, and stained with the anti-SOCS1 antibody for 40 min at RT. After washing, cells were stained with a rabbit anti-mouse AF488 secondary antibody (cat. #31584; Life Technologies; 1:500) for 40–60 min at RT, washed, and analyzed immediately.

### MDA5 and TLR3 assessment

Cells were stained with anti-cMPL and anti-CD34 antibodies, washed, and fixed in 40% methanol at RT for 15 min. Cells were

then washed and permeabilized using 0.1% T-PBS for 15 min at RT. After washing, cells were treated with 1% BSA and 22.52 mg/ml glycine in 0.1% PBS-Tween20 for 30 min at RT, washed, and stained with anti-MDA5 or anti-TLR3 antibodies in 1% BSA/1× PBS at RT for 40 min. After washing, cells are stained with a rabbit anti-mouse AF488 secondary antibody (cat. #31584; Life Technologies; 1:1,500) for 40–60 min at RT, washed, and analyzed immediately.

### IFNβ detection

MNC were treated as indicated for 30 min at 37°C. Monensin (Golgi Stop; BD Biosciences) was added to the cultures, and the cells were once again incubated for 30 min. Cells were washed and stained with anti-CD34 PB and anti-cMPL PE for 15 min on ice light protected. Cells were then fixed with BD Cytofix/Cytoperm buffer (BD Biosciences) for 20 min on ice, washed twice, and permeabilized in BD Perm/Wash buffer (BD Biosciences) for 15 min at RT. Cells were stained with anti-IFNβ FITC antibody (1:100) for 30 min on ice and light protected, subsequently washed, and analyzed immediately.

### 5mC quantification

MNC were fixed using BD cytofix/cytoperm (BD Biosciences) for 20 min on ice. Cells were washed twice with 1× PBS and permeabilized with BD perm/wash buffer (BD Biosciences) for 15 min at RT. Nucleic acid bound to proteins is released by proteinase K treatment for 1 h at 37°C. After washing twice, cells are incubated for up to 1 h at 37°C with Turbo DNase I (cat. # AM1907; Thermo Fisher Scientific) for the digestion of DNA (determination of 5mC in RNA) or with RNase A (cat. # 19101; Qiagen) for digestion of RNA (determination of 5mC in DNA). Cells were washed twice with BD perm/wash buffer and stained with an anti-5mC primary antibody (Abnova) for 30 min on ice. After washing, cells were stained with anti-rabbit Alexa Fluor 488 (Life technologies) secondary antibody (1:500) in 1× PBS at RT for 30 min, washed, and analyzed.

### dsRNA detection by immunofluorescence

Cells were cytospun onto poly-L-lysine coated slides (cat. #67–762; Thermo Fisher Scientific) and fixed in 3.7% paraformaldehyde (cat. #BM1585; Thermo Fisher Scientific), permeabilized with 1× PBS containing 0.2% Triton X-100 (cat. #MTX15681; Thermo Fisher Scientific) for 5 min at RT, and washed with 1× PBS at RT three times for 5 min each time. Cells were then incubated with 20 µg/ml proteinase K (cat. #P9107; New England Biolabs), in 50 mM Tris-HCl, pH 8.0, and 5 mM CaCl$_2$ for 1 h at 37°C. For RNase III digestion, the slides were washed twice and incubated in RNase III (cat# AM2290; Invitrogen) at least 30 min after proteinase K treatments. Primary antibodies against dsRNA (9D5 or J2; Table S8) were incubated overnight at 4°C (diluted 1:100 in 1× PBS), washed three times at RT for 5 min each time in PBS before incubation with a rabbit anti-mouse AF488 secondary antibody (cat. #31584; Life Technologies)

for 30 min, and counterstained with 1 µg/ml DAPI (cat. #10236276001; Millipore Sigma) in 1× PBS for 3 min at RT. Slides were washed once with 1× PBS containing 0.05% Triton X-100 for 5 min each time at RT, twice with 1× PBS for 5 min each time, and once with distilled $H_2O$ for 1 min. Cells were mounted with Prolong Gold antifade gel mount (cat. #P36930; Thermo Fisher Scientific) and imaged on a Cytation 5 inverted fluorescent microscope (BioTek).

### ELISA
MNCs from healthy donors or patients were serum-starved in plain STEM SPAN for 1–2 h and then subjected to treatment for 1 h. IFNα secreted into the cell culture supernatant of primary cells was measured using the Verikine-HS Human IFNα ELISA kit (cat. #41115; PBL Assay Science) according to the manufacturer's instructions.

### Western blotting
Cells were lysed with 50 mM Tris·HCl (pH 7.6) containing 1% NP40, 30 mM NaCl, 1 mM EDTA, 150 mM NaCl, and 1× proteinase inhibitor cocktail (cat. # 4693159001; Millipore Sigma) or RIPA buffer supplemented with EDTA-free protease inhibitor cocktail (11873580001; Sigma-Aldrich) and 1 mM PMSF. Protein concentrations were determined using Protein Assay Kit (5000002; Bio-Rad). Lysates were resolved on 10% NUPAGE Bis-Tris gels (Invitrogen), transferred to polyvinylidene fluoride membranes, and incubated with the relevant antibodies. Stained membrane signals were visualized by using Hyglo HRP detection kit (cat. # E2500; Denville Scientific) and exposed to HyBlot CL film (cat. # E3012; Denville Scientific) by LICOR Odyssey Fc (LI-COR Biosciences). Protein levels were quantified using ImageJ (https://imagej.nih.gov/ij/). Details on antibodies used are listed in Table S8.

### RNA extraction and reverse transcription
Total RNA was extracted from cells using the RNeasy Mini kit (Qiagen) according to the manufacturer's protocol. RNA concentrations were assessed using a Nanodrop 1000 spectrophotometer (Thermo Fisher Scientific). RNA integrity was assessed using a 2100 Bioanalyzer (Agilent) when needed. RNA was reverse transcribed using the SuperScript II (cat. # 18064014; Thermo Fisher Scientific) along with random primers (cat. # 48190011; Thermo Fisher Scientific) according to the manufacturer's recommendations.

### qRT-PCR analysis
Quantitative RT-PCR assays were performed in technical triplicates using the SYBR Green chemistry (cat. #4309155; Thermo Fisher Scientific) on a ViiA 7 Real-Time PCR System (Thermo Fisher Scientific) under standard cycling conditions with melting curve analysis. Expression values were efficiency corrected using the Pfaffl method (Pfaffl, 2001). Relative expression values of target genes were normalized to GAPDH expression. Detailed information on the primers utilized is listed in Table S9.

### Gene expression analysis by microarray
RNA isolated from FACS-sorted MPL+ MNC after treatment for 16 h was amplified and cRNA converted to sense-strand DNA

using the Clariom D Pico Assay (cat. #902924; Thermo Fisher Scientific). The product was hybridized using the GeneChip Hybridization Kit (cat. # 900454; Thermo Fisher Scientific) onto Clariom D Assays, human (cat. # 902922; Thermo Fisher Scientific). The array image was generated using a GeneArray Scanner 3000 7 G (Thermo Fisher Scientific). Following RMA normalization, differentially expressed genes (fold change 1.2 and P value <0.05) were evaluated using the transcriptome analysis console software (Thermo Fisher Scientific). Ingenuity pathway analysis (IPA; Ingenuity Systems), EnrichR (Kuleshov et al., 2016), and GSEA (Broad Institute) software packages were used to further evaluate the differentially expressed genes and dysregulated pathways.

### Analysis of expression of transposable elements (TEs)
TEs can be embedded within gene bodies, correlating with adjacent gene expression (Jordan et al., 2003; Wang et al., 2013). To quantify TE expression, we identified TE-associated genes (based on their locus information) in the reference genome and subsequently quantified differential gene expression between AZA and control-treated cells. We also quantified and compared the number of TE in 679 differentially expressed genes in MPL+ MNC exposed to AZA (vs. mock controls) and 100× randomly sampled transcripts.

### Gene expression analysis by RNA sequencing (RNA-seq)
RNA was depleted of ribosomal RNA (Ribo-Zero rRNA Removal Kit; Epicentre), purified (RNeasy Clean-up Kit; Qiagen), and reverse transcribed to double-stranded cDNA (SuperScript Double-Stranded cDNA Synthesis Kit; Thermo Fisher Scientific). RNA-seq library preparation was performed according to manufacturer's instructions using Illumina compatible ScriptSeq/TruSeq, size-selected, and purified (QIAquick Gel Extraction kit; Qiagen). Transcriptomes were sequenced with the Illumina HiSeq2000 platform using the TruSeq SBS Kit v3-HS reagent kit for paired-end sequencing with 100 bp read length. Reads were corrected with Trimmomatic and after filtering, aligned to the human genome (GRCH38) using STAR and EnsEMBL v82 gene models. Picard was used for sorting aligned reads and marking PCR duplicates. Gene expression was assessed by RNA-seq of BM MNCs extracted from AML patients (N = 7) before and after exposure to AZA treatment. Description of patients and patient sample characteristics, including exposure time to treatment and sampling time after last exposure, is available in Table S5. Differential expression analysis was performed using edgeR (McCarthy et al., 2012) and limma Bioconductor packages (Ritchie et al., 2015). The gene list was subsequently ranked according to the log fold-change (logFC) parameter. The ranked gene list was run in the GSEAPreranked module of GenePattern against MsigDB collections of pathways for the identification of significantly enriched pathways.

### Statistics
The statistical significance of the difference between two groups of paired and unpaired samples was assessed by two-tailed Student's t test, Kolmogorov–Smirnov test, or Welch's t test as indicated in the figure legends. Prism 8.3.0 (GraphPad Software)

or Microsoft Excel was used for statistical analyses and/or plotting of graphs. Differential expression analysis was performed with transcriptome analysis console software.

### Online supplemental material

Fig. S1 shows AZA dose finding, effects of AZA on myeloid progenitors, and details on ex vivo megakaryopoiesis in the presence of AZA. Table S1 lists patient information on the primary cell specimen (Einstein cohort). Table S2 contains a list of differentially expressed genes in MPL expressing MNC after AZA exposure. Table S3 shows the list of significantly enriched gene signatures in MPL⁺ MNC after AZA treatment. Table S4 holds the list of upregulated genes after AZA treatment also enriched in GSE40666. Fig. S2 contains information on dsRNA, 5mC (RNA and DNA) quantification in stem and progenitor cells in megakaryopoiesis, inducing cultures in the presence of AZA or DEC, as well as details on innate immune activation. Fig. S3 depicts details on IFNAR presentation and downstream signaling upon ex vivo or in vivo exposure of HSCP to AZA. Table S5 contains the details for longitudinally sampled AZA treated MDS/AML patients (FIMM cohort). Table S6 contains a list of genes enriched and positively correlated post-AZA treatment in GO negative regulation of Mk differentiation. Table S7 lists genes enriched and positively correlated post-AZA treatment in Hallmark—IFNα response. Fig. S4 holds information on phosphoflow-based strategy to quantify TPO-R signaling in HSPC and MNC exposed to AZA or recombinant IFNα. Fig. S5 shows the model and experimental details on RNAi-mediated SOCS1 knock-down in primary HPSC and contains the proposed mechanistic model supported by the study. Table S8 lists details for antibodies, and Table S9 contains information on primers used in the study.

### Data availability

All data associated with this study are present in the paper or the supplemental material. Gene expression microarray data for this study have been deposited in the Gene Expression Omnibus database with accession number GSE144410.

Author contributions: B. Will designed the study; U.C. Okoye-Okafor and B. Will designed the experiments; U.C. Okoye-Okafor, K.K. Javarappa, D. Tsallos, J. Saad, D. Yang, C. Zhang, L. Benard, V.J. Thiruthuvanathan, S. Cole, S. Ruiz, M. Tatiparthy, G. Choudhary, and S. DeFronzo performed the experiments; U.C. Okoye-Okafor, C. Zhang, and B.A. Bartholdy performed computational analysis; U.C. Okoye-Okafor assembled the data; U.C. Okoye-Okafor, K.K. Javarappa, D. Tsallos, J. Saad, D. Yhang, C. Zhang, A. Verma, A. Shastri, C. Pallaud, P.M. Ramos, C.A. Heckman, and B. Will analyzed and interpreted the data; A. Verma and A. Shastri provided patient samples; C. Pallaud, and P.M. Ramos provided materials; U.C. Okoye-Okafor and B. Will wrote the manuscript; and all authors gave final approval of the manuscript and agreed to be accountable for all aspects of the work.

## References

Abramovich, C., L.M. Shulman, E. Ratovitski, S. Harroch, M. Tovey, P. Eid, and M. Revel. 1994. Differential tyrosine phosphorylation of the IFNAR chain of the type I interferon receptor and of an associated surface protein in response to IFN-alpha and IFN-beta. *EMBO J.* 13:5871–5877. https://doi.org/10.1002/j.1460-2075.1994.tb06932.x

Alcami, A., J.A. Symons, and G.L. Smith. 2000. The vaccinia virus soluble alpha/beta interferon (IFN) receptor binds to the cell surface and protects cells from the antiviral effects of IFN. *J. Virol.* 74:11230–11239. https://doi.org/10.1128/jvi.74.23.11230-11239.2000

Aparicio, A., and J.S. Weber. 2002. Review of the clinical experience with 5-azacytidine and 5-aza-2′-deoxycytidine in solid tumors. *Curr. Opin. Investig. Drugs.* 3:627–633

Bachegowda, L., K. Morrone, S.L. Winski, I. Mantzaris, M. Bartenstein, N. Ramachandra, O. Giricz, V. Sukrithan, G. Nwankwo, S. Shahnaz, et al. 2016. Pexmetinib: A novel dual inhibitor of Tie2 and p38 MAPK with efficacy in preclinical models of myelodysplastic syndromes and acute myeloid leukemia. *Cancer Res.* 76:4841–4849. https://doi.org/10.1158/0008-5472.CAN-15-3062

Benjamin, R., A. Khwaja, N. Singh, J. McIntosh, A. Meager, M. Wadhwa, C. Streck, C. Ng, A.M. Davidoff, and A.C. Nathwani. 2007. Continuous delivery of human type I interferons (alpha/beta) has significant activity against acute myeloid leukemia cells in vitro and in a xenograft model. *Blood.* 109:1244–1247. https://doi.org/10.1182/blood-2006-02-002915

Bromberg, J.F., C.M. Horvath, Z. Wen, R.D. Schreiber, and J.E. Darnell Jr. 1996. Transcriptionally active Stat1 is required for the antiproliferative effects of both interferon alpha and interferon gamma. *Proc. Natl. Acad. Sci. USA.* 93:7673–7678. https://doi.org/10.1073/pnas.93.15.7673

Cheng, J.X., L. Chen, Y. Li, A. Cloe, M. Yue, J. Wei, K.A. Watanabe, J.M. Shammo, J. Anastasi, Q.J. Shen, et al. 2018. Author correction: RNA cytosine methylation and methyltransferases mediate chromatin organization and 5-azacytidine response and resistance in leukaemia. *Nat. Commun.* 9:2286. https://doi.org/10.1038/s41467-018-04518-9

Chiappinelli, K.B., P.L. Strissel, A. Desrichard, H. Li, C. Henke, B. Akman, A. Hein, N.S. Rote, L.M. Cope, A. Snyder, et al. 2015. Inhibiting DNA methylation causes an interferon response in cancer via dsRNA including endogenous retroviruses. *Cell.* 162:974–986. https://doi.org/10.1016/j.cell.2015.07.011

Christman, J.K., N. Mendelsohn, D. Herzog, and N. Schneiderman. 1983. Effect of 5-azacytidine on differentiation and DNA methylation in human promyelocytic leukemia cells (HL-60). *Cancer Res.* 43:763–769

Clark, K., L. Plater, M. Peggie, and P. Cohen. 2009. Use of the pharmacological inhibitor BX795 to study the regulation and physiological roles of TBK1 and IkappaB kinase epsilon: A distinct upstream kinase mediates Ser-172 phosphorylation and activation. *J. Biol. Chem.* 284:14136–14146. https://doi.org/10.1074/jbc.M109.000414

Colamonici, O., H. Yan, P. Domanski, R. Handa, D. Smalley, J. Mullersman, M. Witte, K. Krishnan, and J. Krolewski. 1994. Direct binding to and tyrosine phosphorylation of the alpha subunit of the type I interferon receptor by p135tyk2 tyrosine kinase. *Mol. Cell. Biol.* 14:8133–8142. https://doi.org/10.1128/mcb.14.12.8133-8142.1994

de Sauvage, F.J., K. Carver-Moore, S.M. Luoh, A. Ryan, M. Dowd, D.L. Eaton, and M.W. Moore. 1996. Physiological regulation of early and late stages of megakaryocytopoiesis by thrombopoietin. *J. Exp. Med.* 183:651–656. https://doi.org/10.1084/jem.183.2.651

de Swart, L., A. Smith, T.W. Johnston, D. Haase, P. Fenaux, A. Symeonidis, G. Sanz, E. Hellstrom-Lindberg, J. Cermak, et al. 2015. Validation of the revised international prognostic scoring system (IPSS-R) in patients with lower-risk myelodysplastic syndromes: A report from the prospective European LeukaemiaNet MDS (EUMDS) registry. *Br. J. Haematol.* 170:372–383. https://doi.org/10.1111/bjh.13450

Dickinson, M., H. Cherif, P. Fenaux, M. Mittelman, A. Verma, M.S.O. Portella, P. Burgess, P.M. Ramos, J. Choi, U. Platzbecker, and SUPPORT study investigators. 2018. Azacitidine with or without eltrombopag for first-line treatment of intermediate- or high-risk MDS with thrombocytopenia. *Blood.* 132:2629–2638. https://doi.org/10.1182/blood-2018-06-855221

El Hajjar, J., W. Chatoo, R. Hanna, P. Nkanza, N. Tétreault, Y.C. Tse, T.P. Wong, M. Abdouh, and G. Bernier. 2019. Heterochromatic genome instability and neurodegeneration sharing similarities with Alzheimer's disease in old Bmi1+/- mice. *Sci. Rep.* 9:594. https://doi.org/10.1038/s41598-018-37444-3

Endo, T.A., M. Masuhara, M. Yokouchi, R. Suzuki, H. Sakamoto, K. Mitsui, A. Matsumoto, S. Tanimura, M. Ohtsubo, H. Misawa, et al. 1997. A new protein containing an SH2 domain that inhibits JAK kinases. *Nature.* 387:921–924. https://doi.org/10.1038/43213

Erickson-Miller, C.L., E. Delorme, S.S. Tian, C.B. Hopson, A.J. Landis, E.I. Valoret, T.S. Sellers, J. Rosen, S.G. Miller, J.I. Luengo, et al. 2009. Preclinical activity of eltrombopag (SB-497115), an oral, nonpeptide thrombopoietin receptor agonist. *Stem Cells.* 27:424–430. https://doi.org/10.1634/stemcells.2008-0366

Essers, M.A., S. Offner, W.E. Blanco-Bose, Z. Waibler, U. Kalinke, M.A. Duchosal, and A. Trumpp. 2009. IFNalpha activates dormant haematopoietic stem cells in vivo. *Nature.* 458:904–908. https://doi.org/10.1038/nature07815

Farmer, L.J., M.W. Ledeboer, T. Hoock, M.J. Arnost, R.S. Bethiel, Y.L. Bennani, J.J. Black, C.L. Brummel, A. Chakilam, W.A. Dorsch, et al. 2015. Discovery of VX-509 (Decernotinib): A potent and selective Janus kinase 3 inhibitor for the treatment of autoimmune diseases. *J. Med. Chem.* 58: 7195–7216. https://doi.org/10.1021/acs.jmedchem.5b00301

Fenaux, P., G.J. Mufti, E. Hellstrom-Lindberg, V. Santini, C. Finelli, A. Giagounidis, R. Schoch, N. Gattermann, G. Sanz, A. List, et al. 2009. Efficacy of azacitidine compared with that of conventional care regimens in the treatment of higher-risk myelodysplastic syndromes: A randomised, open-label, phase III study. *Lancet Oncol.* 10:223–232. https://doi.org/10.1016/S1470-2045(09)70003-8

Fitzgerald, K.A., S.M. McWhirter, K.L. Faia, D.C. Rowe, E. Latz, D.T. Golenbock, A.J. Coyle, S.M. Liao, and T. Maniatis. 2003. IKKepsilon and TBK1 are essential components of the IRF3 signaling pathway. *Nat. Immunol.* 4:491–496. https://doi.org/10.1038/ni921

Gantier, M.P., and B.R. Williams. 2007. The response of mammalian cells to double-stranded RNA. *Cytokine Growth Factor Rev.* 18:363–371. https://doi.org/10.1016/j.cytogfr.2007.06.016

Garcia-Manero, G., H.J. Khoury, E. Jabbour, J. Lancet, S.L. Winski, L. Cable, S. Rush, L. Maloney, G. Hogeland, M. Ptaszynski, et al. 2015. A phase I study of oral ARRY-614, a p38 MAPK/Tie2 dual inhibitor, in patients with low or intermediate-1 risk myelodysplastic syndromes. *Clin. Cancer Res.* 21:985–994. https://doi.org/10.1158/1078-0432.CCR-14-1765

Haas, S., J. Hansson, D. Klimmeck, D. Loeffler, L. Velten, H. Uckelmann, S. Wurzer, A.M. Prendergast, A. Schnell, K. Hexel, et al. 2015. Inflammation-induced emergency megakaryopoiesis driven by hematopoietic stem cell-like megakaryocyte progenitors. *Cell Stem Cell.* 17: 422–434. https://doi.org/10.1016/j.stem.2015.07.007

Izquierdo-Bouldstridge, A., A. Bustillos, C. Bonet-Costa, P. Aribau-Miralbés, D. García-Gomis, M. Dabad, A. Esteve-Codina, L. Pascual-Reguant, S. Peiró, M. Esteller, et al. 2017. Histone H1 depletion triggers an interferon response in cancer cells via activation of heterochromatic repeats. *Nucleic Acids Res.* 45:11622–11642. https://doi.org/10.1093/nar/gkx746

Jordan, I.K., I.B. Rogozin, G.V. Glazko, and E.V. Koonin. 2003. Origin of a substantial fraction of human regulatory sequences from transposable elements. *Trends Genet.* 19:68–72. https://doi.org/10.1016/s0168-9525(02)00006-9

Kantarjian, H., F. Giles, A. List, R. Lyons, M.A. Sekeres, S. Pierce, R. Deuson, and J. Leveque. 2007. The incidence and impact of thrombocytopenia in myelodysplastic syndromes. *Cancer.* 109:1705–1714. https://doi.org/10.1002/cncr.22602

Karjalainen, R., T. Pemovska, M. Popa, M. Liu, K.K. Javarappa, M.M. Majumder, B. Yadav, D. Tamborero, J. Tang, D. Bychkov, et al. 2017. JAK1/2 and BCL2 inhibitors synergize to counteract bone marrow stromal cell-induced protection of AML. *Blood.* 130:789–802. https://doi.org/10.1182/blood-2016-02-699363

Kaushansky, K. 2005. The molecular mechanisms that control thrombopoiesis. *J. Clin. Invest.* 115:3339–3347. https://doi.org/10.1172/JCI26674

Kuleshov, M.V., M.R. Jones, A.D. Rouillard, N.F. Fernandez, Q. Duan, Z. Wang, S. Koplev, S.L. Jenkins, K.M. Jagodnik, A. Lachmann, et al. 2016. Enrichr: a comprehensive gene set enrichment analysis web server 2016 update. *Nucleic Acids Res.* 44:W90-7. https://doi.org/10.1093/nar/gkw377

Kuter, D.J. 2009. Thrombopoietin and thrombopoietin mimetics in the treatment of thrombocytopenia. *Annu. Rev. Med.* 60:193–206. https://doi.org/10.1146/annurev.med.60.042307.181154

Lee, H.C., E.S. Lee, M.B. Uddin, T.H. Kim, J.H. Kim, K. Chathuranga, W.A.G. Chathuranga, M. Jin, S. Kim, C.J. Kim, and J.S. Lee. 2019. Released tryptophanyl-tRNA Synthetase stimulates innate immune responses against viral infection. *J. Virol.* 93:e01291-18. https://doi.org/10.1128/JVI.01291-18

Li, X., S. Leung, I.M. Kerr, and G.R. Stark. 1997. Functional subdomains of STAT2 required for preassociation with the alpha interferon receptor and for signaling. *Mol. Cell. Biol.* 17:2048–2056. https://doi.org/10.1128/MCB.17.4.2048

Li, H., K.B. Chiappinelli, A.A. Guzzetta, H. Easwaran, R.W. Yen, R. Vatapalli, M.J. Topper, J. Luo, R.M. Connolly, N.S. Azad, et al. 2014. Immune regulation by low doses of the DNA methyltransferase inhibitor 5-azacitidine in common human epithelial cancers. *Oncotarget.* 5: 587–598. https://doi.org/10.18632/oncotarget.1782

Mattia, G., F. Vulcano, L. Milazzo, A. Barca, G. Macioce, A. Giampaolo, and H.J. Hassan. 2002. Different ploidy levels of megakaryocytes generated from peripheral or cord blood CD34+ cells are correlated with different levels of platelet release. *Blood.* 99:888–897. https://doi.org/10.1182/blood.v99.3.888

Mayer, I.A., A. Verma, I.M. Grumbach, S. Uddin, F. Lekmine, F. Ravandi, B. Majchrzak, S. Fujita, E.N. Fish, and L.C. Platanias. 2001. The p38 MAPK pathway mediates the growth inhibitory effects of interferon-alpha in BCR-ABL-expressing cells. *J. Biol. Chem.* 276:28570–28577. https://doi.org/10.1074/jbc.M011685200

Mazur, E.M., W.J. Richtsmeier, and K. South. 1986. Alpha-interferon: Differential suppression of colony growth from human erythroid, myeloid, and megakaryocytic hematopoietic progenitor cells. *J. Interferon Res.* 6: 199–206. https://doi.org/10.1089/jir.1986.6.199

McCarthy, D.J., Y. Chen, and G.K. Smyth. 2012. Differential expression analysis of multifactor RNA-Seq experiments with respect to biological variation. *Nucleic Acids Res.* 40:4288–4297. https://doi.org/10.1093/nar/gks042

McCullough, J. 2000. Current issues with platelet transfusion in patients with cancer. *Semin. Hematol.* 37:3–10. https://doi.org/10.1016/s0037-1963(00)90047-7

National Comprehensive Cancer Network. 2017. NCCN Clinical Practice Guidelines in Oncology: Myelodysplastic Syndromes

Neukirchen, J., S. Blum, A. Kuendgen, C. Strupp, M. Aivado, R. Haas, C. Aul, N. Gattermann, and U. Germing. 2009. Platelet counts and haemorrhagic diathesis in patients with myelodysplastic syndromes. *Eur. J. Haematol.* 83:477–482. https://doi.org/10.1111/j.1600-0609.2009.01299.x

Olnes, M.J., P. Scheinberg, K.R. Calvo, R. Desmond, Y. Tang, B. Dumitriu, A.R. Parikh, S. Soto, A. Biancotto, X. Feng, et al. 2012. Eltrombopag and improved hematopoiesis in refractory aplastic anemia. *N. Engl. J. Med.* 367:11–19. https://doi.org/10.1056/NEJMoa1200931

Pfaffl, M.W. 2001. A new mathematical model for relative quantification in real-time RT-PCR. *Nucleic Acids Res.* 29:e45. https://doi.org/10.1093/nar/29.9.e45

Piganis, R.A.R., N.A. De Weerd, J.A. Gould, C.W. Schindler, A. Mansell, S.E. Nicholson, and P.J. Hertzog. 2011. Suppressor of cytokine signaling (SOCS) 1 inhibits type I interferon (IFN) signaling via the interferon alpha receptor (IFNAR1)-associated tyrosine kinase Tyk2. *J. Biol. Chem.* 286:33811–33818. https://doi.org/10.1074/jbc.M111.270207

Reckhaus, J., M. Jutzi, S. Fontana, V.U. Bacher, M. Vogt, M. Daslakis, and B. Mansouri Taleghani. 2018. Platelet transfusion induces alloimmunization to D and non-D rhesus antigens. *Transfus. Med. hemotherapy*. 45:167–172. https://doi.org/10.1159/000490122

Ritchie, M.E., B. Phipson, D. Wu, Y. Hu, C.W. Law, W. Shi, and G.K. Smyth. 2015. limma powers differential expression analyses for RNA-sequencing and microarray studies. *Nucleic Acids Res.* 43:e47. https://doi.org/10.1093/nar/gkv007

Roulois, D., H. Loo Yau, R. Singhania, Y. Wang, A. Danesh, S.Y. Shen, H. Han, G. Liang, P.A. Jones, T.J. Pugh, et al. 2015. DNA-demethylating agents target colorectal cancer cells by inducing viral mimicry by endogenous transcripts. *Cell*. 162:961–973. https://doi.org/10.1016/j.cell.2015.07.056

Schaefer, M., S. Hagemann, K. Hanna, and F. Lyko. 2009. Azacytidine inhibits RNA methylation at DNMT2 target sites in human cancer cell lines. *Cancer Res.* 69:8127–8132. https://doi.org/10.1158/0008-5472.CAN-09-0458

Schaefer, M., T. Pollex, K. Hanna, F. Tuorto, M. Meusburger, M. Helm, and F. Lyko. 2010. RNA methylation by Dnmt2 protects transfer RNAs against stress-induced cleavage. *Genes Dev.* 24:1590–1595. https://doi.org/10.1101/gad.586710

Stark, G.R., and J.E. Darnell Jr. 2012. The JAK-STAT pathway at twenty. *Immunity*. 36:503–514. https://doi.org/10.1016/j.immuni.2012.03.013

Stone, M.L., K.B. Chiappinelli, H. Li, L.M. Murphy, M.E. Travers, M.J. Topper, D. Mathios, M. Lim, I.M. Shih, T.L. Wang, et al. 2017. Epigenetic therapy activates type I interferon signaling in murine ovarian cancer to reduce immunosuppression and tumor burden. *Proc. Natl. Acad. Sci. USA*. 114:E10981–E10990. https://doi.org/10.1073/pnas.1712514114

Svensson, T., O. Chowdhury, H. Garelius, F. Lorenz, L. Saft, S.E. Jacobsen, E. Hellstrom-Lindberg, and H. Cherif. 2014. A pilot phase I dose finding safety study of the thrombopoietin-receptor agonist, eltrombopag, in patients with myelodysplastic syndrome treated with azacitidine. *Eur. J. Haematol.* 93:439–445. https://doi.org/10.1111/ejh.12383

Symons, J.A., A. Alcami, and G.L. Smith. 1995. Vaccinia virus encodes a soluble type I interferon receptor of novel structure and broad species specificity. *Cell*. 81:551–560. https://doi.org/10.1016/0092-8674(95)90076-4

van den Bosch, J., M. Lubbert, G. Verhoef, and P.W. Wijermans. 2004. The effects of 5-aza-2'-deoxycytidine (Decitabine) on the platelet count in patients with intermediate and high-risk myelodysplastic syndromes. *Leuk. Res.* 28:785–790. https://doi.org/10.1016/j.leukres.2003.11.016

Wang, Q., Y. Miyakawa, N. Fox, and K. Kaushansky. 2000. Interferon-alpha directly represses megakaryopoiesis by inhibiting thrombopoietin-induced signaling through induction of SOCS-1. *Blood*. 96:2093–2099

Wang, B., J.L. Nichol, and J.T. Sullivan. 2004. Pharmacodynamics and pharmacokinetics of AMG 531, a novel thrombopoietin receptor ligand. *Clin. Pharmacol. Ther.* 76:628–638. https://doi.org/10.1016/j.clpt.2004.08.010

Wang, X., D. Weigel, and L.M. Smith. 2013. Transposon variants and their effects on gene expression in Arabidopsis. *PLoS Genet.* 9:e1003255. https://doi.org/10.1371/journal.pgen.1003255

Webb, I.J., and K.C. Anderson. 1999. Risks, costs, and alternatives to platelet transfusions. *Leuk. Lymphoma*. 34:71–84. https://doi.org/10.3109/10428199909083382

Will, B., M. Kawahara, J.P. Luciano, I. Bruns, S. Parekh, C.L. Erickson-Miller, M.A. Aivado, A. Verma, and U. Steidl. 2009. Effect of the nonpeptide thrombopoietin receptor agonist Eltrombopag on bone marrow cells from patients with acute myeloid leukemia and myelodysplastic syndrome. *Blood*. 114:3899–3908. https://doi.org/10.1182/blood-2009-04-219493

Will, B., L. Zhou, T.O. Vogler, S. Ben-Neriah, C. Schinke, R. Tamari, Y. Yu, T.D. Bhagat, S. Bhattacharyya, L. Barreyro, et al. 2012. Stem and progenitor cells in myelodysplastic syndromes show aberrant stage-specific expansion and harbor genetic and epigenetic alterations. *Blood*. 120:2076–2086. https://doi.org/10.1182/blood-2011-12-399683

Yu, M., and A.B. Cantor. 2012. Megakaryopoiesis and thrombopoiesis: An update on cytokines and lineage surface markers. *Methods Mol. Biol.* 788:291–303. https://doi.org/10.1007/978-1-61779-307-3_20

Zhang, X.H., L. Yang, X.J. Liu, Y. Zhan, Y.X. Pan, X.Z. Wang, and J.M. Luo. 2018. Association between methylation of tumor suppressor gene SOCS1 and acute myeloid leukemia. *Oncol. Rep.* 40:1008–1016. https://doi.org/10.3892/or.2018.6508
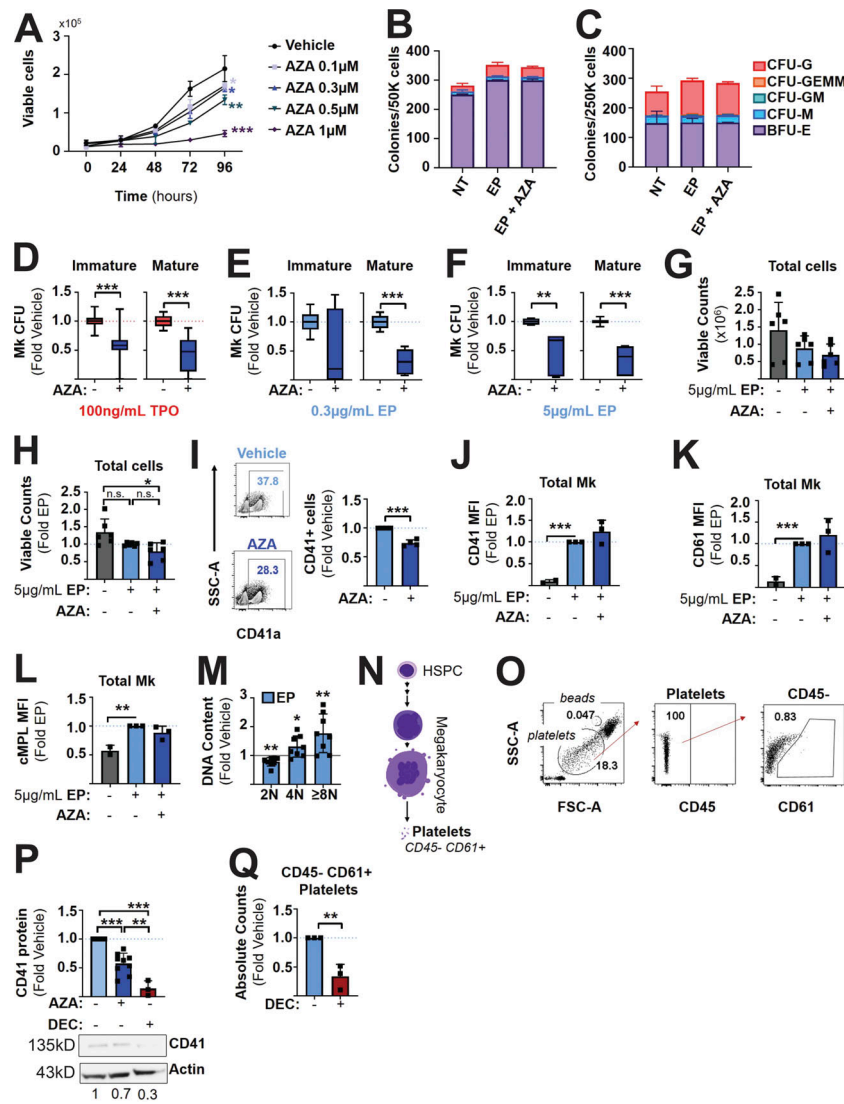
**Figure S1. Decreased Mk cell growth and differentiation upon treatment with AZA or DEC. (A)** Effects of increasing doses of AZA on UKE1 cell growth. Cell viability was quantified by Trypan Blue exclusion following culture of cells for the indicated time points (in hours) in technical replicates. **(B and C)** Quantification of myeloid colony formation of MNC in the presence or absence of AZA. MNC were seeded in Human Methylcellulose Complete Media (R&D; HSC003) either in the absence (no treatment, NT) or presence of 5 µg/ml EP alone, or in addition to 0.3 µM AZA (EP+AZA). Colony formation of healthy volunteer (B) or AML patient–derived BM-MNC (C). Shown are averages and standard deviations of the number of CFU of the granulocytic (CFU-G), granulocytic/erythroid/monocytic/Mk (CFU-GEMM), granulocytic/monocytic (CFU-GM), monocytic (CFU-M) and erythroid lineages (BFU-E). N = 3 biological/group in technical duplicate. **(D–F)** Quantification of immature and mature Mk CFU in healthy control–derived MNC by MegaCult assay (containing TPO [D] or EP [E and F] to stimulate Mk CFU growth) in absence or presence of AZA (0.3 µM). The number of Mk CFU is represented as box plots with min to max (whiskers) and normalized to cultures lacking AZA (containing only TPO or EP, respectively). Mk CFU upon culture in (D) 50–100 ng/ml TPO (N = 7 biological replicates), (E) 0.3 µg/ml EP (N = 4 biological replicates), and (F) 5 µg/ml EP (N = 3 biological replicates). **(G–M)** Assessment of cell growth, differentiation and maturation in liquid Mk differentiation–promoting cultures (containing 5 µg/ml EP) in the absence and presence of AZA (0.3 µM) at culture day 14. **(G and H)** Cell viability by Trypan Blue exclusion counting, absolute counts (G) and expressed as fold changes compared with EP treatment controls (H); N = 3 independent biological samples. **(I)** Representative FACS contour plots of CD41a-expressing (CD41⁺) cells (left). Bar graphs depict means ± SD of relative frequencies of CD41⁺ cells of as fold changes compared with EP containing cultures lacking AZA (right). N = 4 biological specimen in independent experiments. **(J–L)** Analysis of cell surface markers associated with Mk differentiation and maturation. Means and SD of MFI values of CD41 (J), CD61 (K), and cMPL receptors (L) gated on CD41⁺ cMPL⁺ cells as fold changes compared with EP treatment controls; filled squares show normalized individual data values. N = 3 independent experiments and biological specimens. **(M)** Quantification of DNA content by PI staining in CD41⁺ MNC at day 14 in Mk differentiation–promoting cultures (containing EP) without AZA. CD41⁺ cells were subgated at 2N, 4N, or ≥8N for DNA content, respectively. Bar graphs represent mean ± SD of frequencies of cells in each gate and expressed as fold changes compared with base cultures lacking Mk stimulation (by EP; vehicle, indicated by the black line); filled squares show normalized individual data values. N = 8 biological specimens in independent experiments. **(N)** Schematic of PLT production from HSPCs. **(O)** Representative gating strategy for the evaluation of CD45⁻ CD61⁺ PLTs. **(P)** Quantification of CD41 protein levels by Western blot using CD34⁺ CB cells after 14 d in Mk differentiation stimulating cultures. N = 2–4 biological samples with experimental and technical replicates. Bar graphs depict mean ± SD as fold change of vehicle control. AZA treatment as in Fig. 1 F. **(Q)** Quantification of PLTs (CD45⁻ CD61⁺). Absolute counts determined by manual counting and count beads and expressed as a fold change of vehicle control. N = 3 independent experiments and biological samples. Statistical significance indicated as *P < 0.05, **P < 0.01, ***P < 0.001 by Student's t test; n.s., not significant. Source data are available for this figure: SourceData FS1.
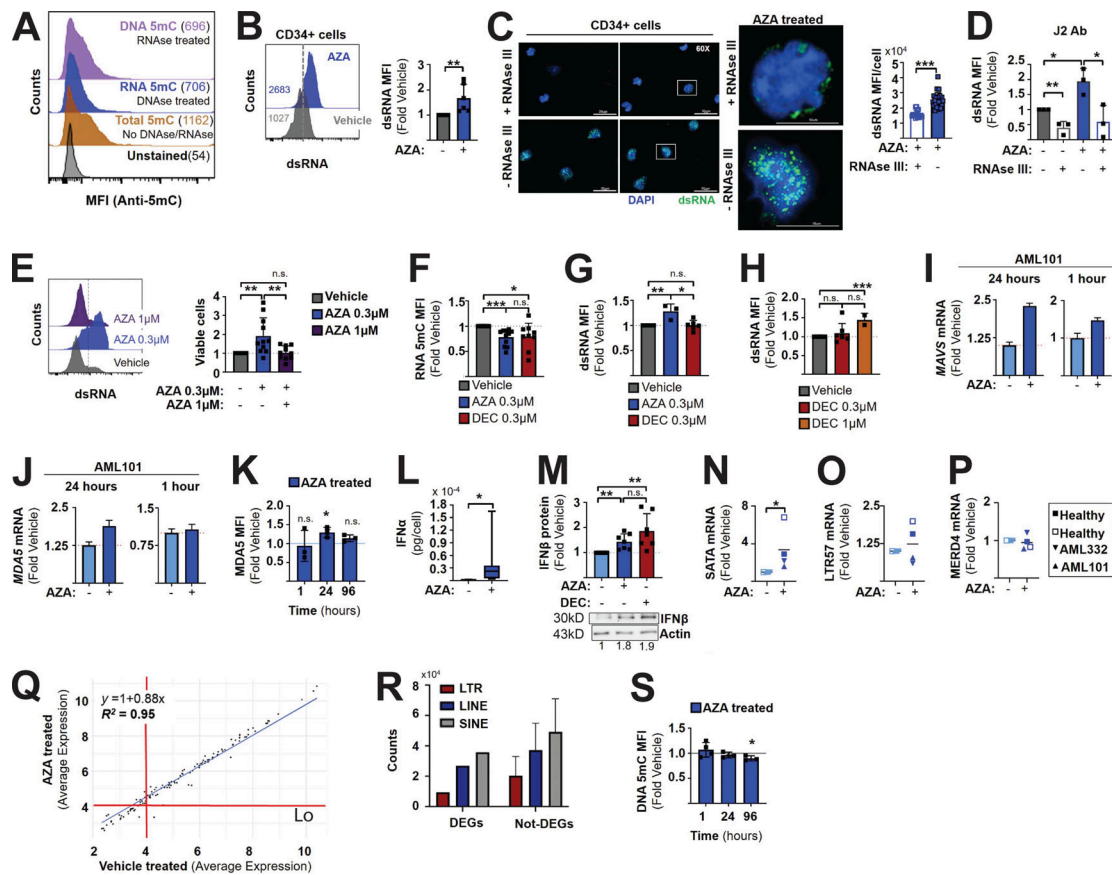
Figure S2. **Induction of dsRNA and ERV-independent activation of IFN-I production upon AZA treatment. (A)** Quantification of 5mC abundance using intracellular FACS analysis. Shown are histograms of MFI of cells stained with an anti-5mC antibody following either single RNAse (top, violet), DNAse (second from top, blue), or no RNAse or DNAse (second from bottom, brown) treatment; unstained cells (bottom, gray) as controls. MFI values are indicated for each control (in parentheses). **(B and C)** Quantification of dsRNA abundance in absence or presence of AZA in CB-derived CD34⁺ cell cultures without TPO-R stimulation by intracellular FACS after 1 h of treatment (B), and immunofluorescence after 30 min of treatment (C). **(B)** Representative FACS histogram (left; control [gray] lacking AZA and AZA-treated [blue] cells; counts normalized to modal) and quantification of MFI (right) normalized to controls devoid of AZA. Bar graphs represent mean ± SD along with individual data points (filled squares). N = 3 independent experiments and biological specimens. **(C)** dsRNA immunofluorescence (green) in contrast to nuclear stain DAPI (blue). Scale bar: 10 μm. CD34⁺ cells treated with AZA and incubated in RNaseIII served as background controls. dsRNA quantification within individual cells MFI as mean ± SD. **(D)** dsRNA abundance in CB-MNC by intracellular FACS analysis. CB-MNC treated in absence (control, gray) or presence of AZA (blue); Bar graphs represent mean ± SD of expression values as fold changes of vehicle; N = 3 independent experiments and biological samples. RNaseIII-treated cells as background controls. **(E)** dsRNA abundance in CB-MNC by intracellular FACS analysis. CB-MNC treated with increasing dose of AZA (0.3 μM, blue; or 1 μM, purple) compared with vehicle control (control, gray). N = 3 biological samples. Bar graphs represent mean ± SD of expression values as fold changes of vehicle control cells. **(F–H)** Evaluation of RNA 5mC and dsRNA changes in DEC-treated MNCs represented as mean ± SD of vehicle controls in the absence or presence of 0.3 μM AZA or DEC (0.3 or 1 μM). RNA 5mC MFI (F); dsRNA MFI (G and H). **(I)** MAVS transcripts by qRT-PCR of AML MNC in the absence or presence of AZA after 24 and 1 h after culture lacking TPO-R–stimulating agents. Bar graphs represent means ± SD of GAPDH normalized relative mRNA expression (arbitrary units) in technical triplicates. **(J)** MDA5 mRNA expression by qRT-PCR after treatment of AML MNC with or without AZA for 24 (left) or 1 h (right). Bar graphs represent means ± SD of GAPDH-normalized relative mRNA expression (arbitrary units) in technical triplicates. **(K)** MDA5 intracellular protein levels quantified by intracellular FACS analysis. Healthy donor MNC cultured for 1, 24, or 96 h in the absence or presence of 0.3 μM AZA in TPO-R stimulating cultures (containing 5 μg/ml EP). Bar graphs represent means ± SD of MDA5 protein levels expressed as fold changes compared with controls (EP); N = 3 independent experiments and biological samples. **(L)** Measurement of secreted IFNα by ELISA in patient-derived MNC in after 1 h in Mk differentiation–stimulating cultures in presence or absence of AZA. IFNα levels are represented as box plots with min to max (whiskers) as pg/cell; N = 6 independent experiments and biological samples. **(M)** IFNβ protein expression within 24 h of treatment in absence (−) or presence (+) of AZA or DEC by Western blot analysis. Bar graphs represent mean protein ± SD normalized to actin loading control. Representative blot displayed. N = 4 independent biological specimens in technical duplicates. AZA-only data displayed in Fig. 3 J. **(N–P)** qRT-PCR of ERV transcripts, SATA (N), LTR57 (O), MERD4 (P) of healthy volunteer and AML patient–derived MNC treated for 24 h with AZA in TPO-R–stimulating cultures (with 5 μg/ml EP). Graph depicts mean expression (black line) for four independent experiments; symbols represent independent samples. **(Q)** Assessment of ERV-associated gene expression correlation in AZA- and control-treated MPL-expressing cells. Shown are expression averages of 125 genes embedded with 189 ERVs as detected by microarray analysis (Fig. 2, A and B). Linear regression model shows the expression of ERV-associated genes is statistically correlated ($R^2$ = 0.95). Red lines indicate genes with detectable expression levels. **(R)** Enrichment analysis of TE (counts) in 679 genes differentially expressed (DEGs) in MPL⁺ MNC exposed to AZA (vs. mock controls) or 100× randomly sampled transcripts (not-DEGs). **(S)** Quantification of DNA 5mC levels in MNC upon 1, 24, and 96 h in culture in the absence or presence of AZA by intracellular FACS analysis. Bar graphs depict means ± SD of MFI normalized to cultures lacking AZA along with individual data points. N = 3–4 independent experiments and biological samples. Statistical significance indicated as *P < 0.05, **P < 0.01, ***P < 0.001 by Student's t test; n.s. or no asterisk, not significant (O, P, and R) or no statistical testing possible as individual specimen were investigated (I and J). Source data are available for this figure: SourceData FS2.
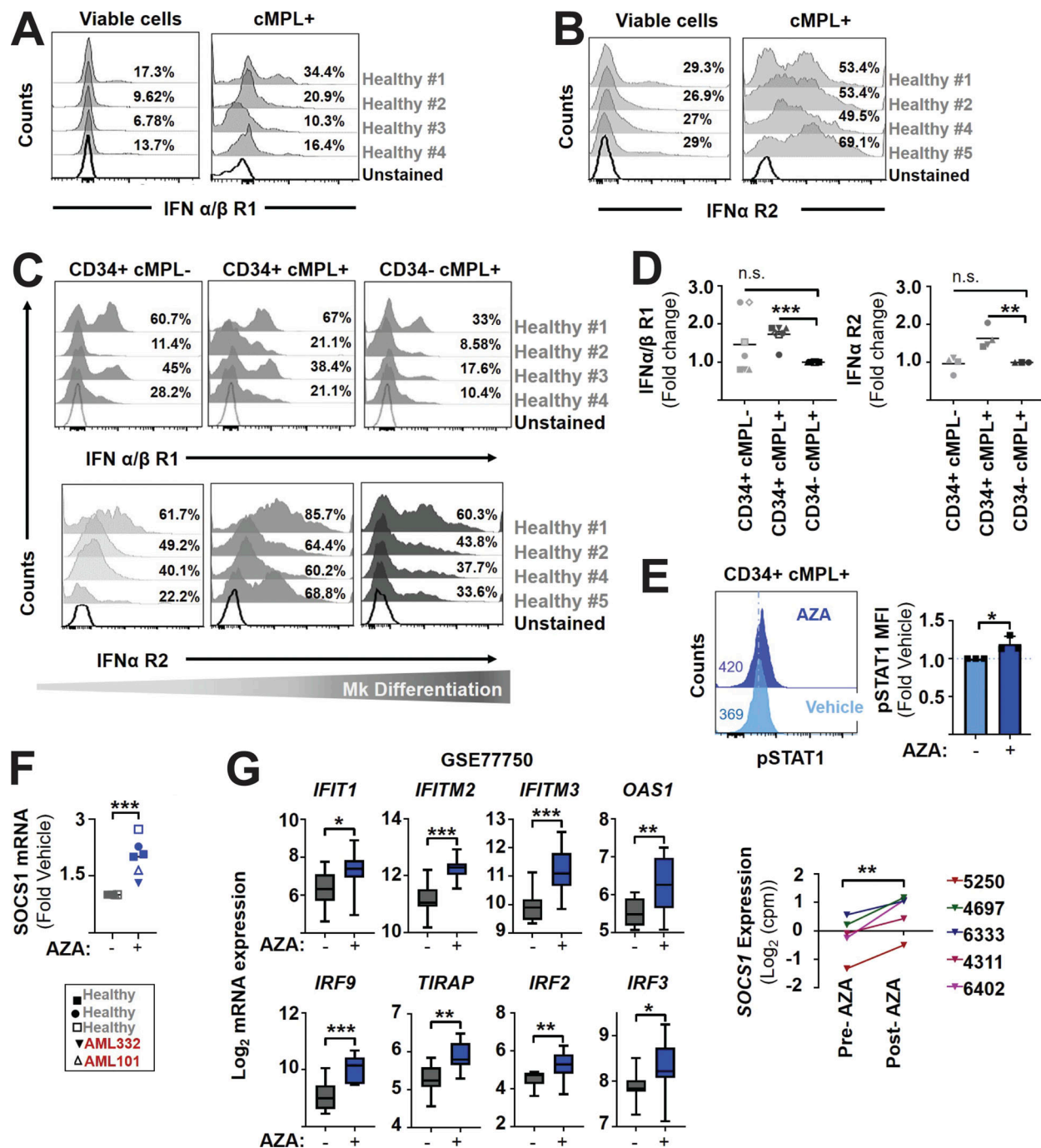
Figure S3. **Differential sensitivity of HSPC to IFN-I activation. (A–D)** Assessment of IFNAR1 and IFNAR2 expressing cells by FACS. **(A and B)** Characterization of IFNAR1 (A) and IFNAR2 (B) expression in healthy donor MNCs (CB- and BM-derived; gated on total viable cells, left; and cMPL+ Mk cells, right). N = 4 biological samples. **(C and D)** Quantification of the number of cells with IFNAR1 and IFNAR2 receptor expression on CD34+ cMPL− immature myeloid cells, CD34+ cMPL+ immature Mk cells, and CD34− cMPL+ mature Mk cells. N = 4 biological samples in independent experiments. Representative FACS plots (C) depict receptor expression in order of increasing Mk differentiation. Graphs (D) show means (black line) and individual data points of percentages of IFNAR-positive cells within purified cell populations) expressed as fold changes compared with the frequency of IFNAR+ cells within CD34− cMPL+ mature Mk cell populations. **(E)** Quantification of phosphorylated STAT1 protein levels by phosphoflow analysis in CD34+ cMPL+ cells. MNC were cultured for 1 h in Mk differentiation cultures (containing 5 µg/ml EP) in the absence or presence of AZA. Representative FACS histogram of pSTAT1 signal in CD34+ cMPL+ cells (left; vehicle control [light blue] and AZA [dark blue]; counts normalized to modal) and quantification of pSTAT1 MFI (right) normalized to vehicle. Bar graphs represent mean ± SD along with individual data points; N = 3 biological samples in independent experiments. **(F)** SOCS1 mRNA by qRT-PCR after a 24 h culture of healthy or AML MNCs in the absence or presence of AZA. Individual data points expressed as fold change vehicle for each sample; N ≥ 5 independent specimen and experiments. **(G)** Expression of IFN-stimulated genes (specified on top of graphs) in CD34+ cells from responders to AZA therapy before and after AZA treatment (GSE77750). Normalized log₂ expression values as box plots (N = 10 [control] and 13 [AZA]). **(H)** Quantification of SOCS1 mRNA expression in paired MDS/AML patient BM-MNC specimen before and after AZA treatment (N = 5). Statistical significance indicated as *P < 0.05, **P < 0.01, ***P < 0.001 by Student's t test (D–G) and Welch's t test (H); n.s., not significant.
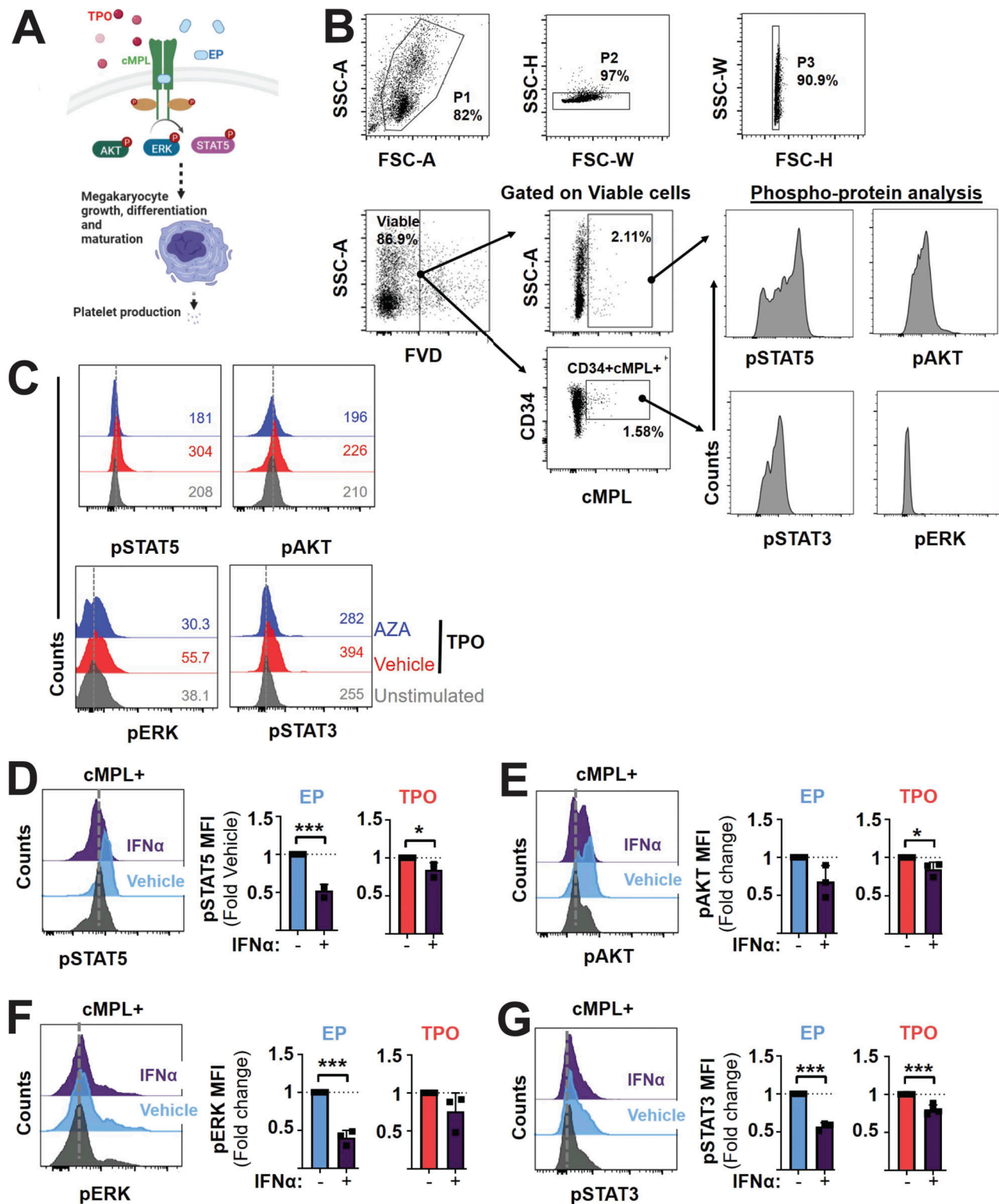
Figure S4. **AZA-mediated impairment of TPO-R signaling can be rescued by inhibition of IFN-I signaling. (A)** Mechanistic scheme of TPO-R/cMPL activation by EP or TPO leading to phosphorylation of STAT5, AKT, and ERK. **(B)** Gating strategy for evaluation of phosphorylated STAT5, STAT3, AKT, and ERK by intracellular phosphoflow. FSC/SSC FVD⁻ (intact, single, viable) cells were subgated for MPL expression. cMPL⁺ cells were analyzed for phospho-STAT5, phospho-AKT, phospho-STAT3, and phospho-ERK1/2. Example histogram plots for a specimen derived from a patient with AML are shown. Background fluorescence from unstained cells (equivalent to isotype controls) are used as negative controls. **(C)** Representative histograms showing counts normalized to modal from healthy donor MNC in vehicle or AZA-treated samples compared with unstimulated control in TPO-R stimulating cultures. **(D–G)** TPO-R downstream signaling in CB MNC stimulated with 5 μg/ml EP or 100 ng/ml TPO (as indicated) in the absence or presence of 10 ng/ml IFNα. N = 3 independent experiments and biological samples. Bar graphs depict mean MFI ± SD of pSTAT5 (D), pAKT (E), pERK (F), and pSTAT3 (G) in MPL⁺ cells normalized to vehicle-treated controls. Statistical significance indicated as *P < 0.05, **P < 0.01, ***P < 0.001 by Student's t test; n.s., not significant.
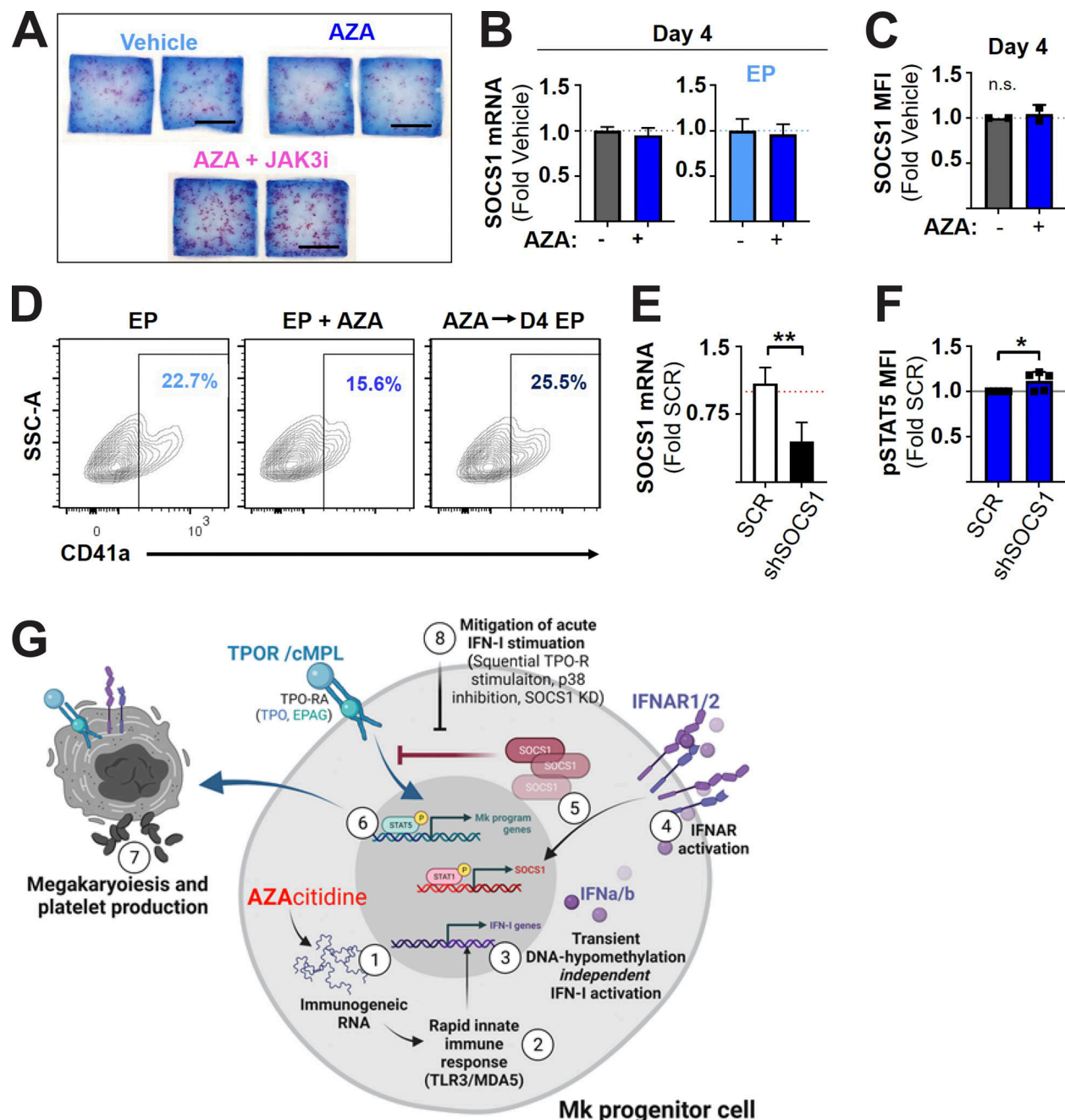
**Figure S5. Inhibition of IFN-I rescues AZA mediated inhibition of megakaryopoiesis. (A)** Representative MegaCult slides following culture of CB-derived MNC (healthy; scale bars indicate 10 mm). **(B)** *SOCS1* mRNA by qRT-PCR upon treatment of healthy MNC treated for 4 d in the absence or presence of AZA in unstimulated cells (gray) or TPO-R stimulating culture containing EP (light blue). Bar graphs represent *GAPDH* normalized relative mRNA expression means (arbitrary units) ± SD normalized to vehicle controls (sample assayed in triplicates). **(C)** Quantification of SOCS1 protein by intracellular FACS of MNC treated for 4 d in the absence or presence of AZA. Bar graphs represent SOCS1 protein mean ± SD normalized to vehicle control for two independent experiments and biological samples. **(D)** Flow cytometry analysis of CD41a-expressing cells after 14 d in Mk-promoting conditions (containing 5 μg/ml EP) in the absence (EP) or presence of 0.3 μM AZA (EP + AZA) or sequentially (AZA → D4 EP). **(E and F)** Downregulation of *SOCS1* by small hairpin (sh)RNA. Lentiviral knockdown in CB-derived cells for 48 h, followed by treatment for 2 h and subsequent phosphoflow analysis of pSTAT5. *N* = 2 independent experiments in technical triplicates. **(F)** pSTAT5 MFI mean ± SD after *SOCS1* knockdown and treatment with AZA calculated as fold-change of scrambled (SCR) control. *N* = 5 independent experiments and biological samples with technical repeats. **(G)** Schematic of molecular mechanism of action proposed by this study. AZA triggers rapid and acute RNA demethylation and accumulation of immunogenic dsRNA species (1), which elicits TLR3/MDA5-dependent innate immune signaling activation (2), including the increase in IFN-I cytokine production and release independent of DNA hypomethylation and the reactivation of ERVs (3) in MNC, including stem and progenitor cells with Mk potential. Cells expressing high levels of functional heterodimeric IFN1R1/2 receptors at their cell surface activate downstream signaling (4), which increases SOCS1 abundance (5) in MNC including stem and progenitor cells with Mk potential. In progenitors with Mk lineage capacity, this leads to the inhibition of TPO-R agonist (endogenous TPO, or small molecule mimetic EP [EPAG])-mediated TPO-R activation (6) and an increase in mega-karyopoiesis and PLT production (7). Mitigation of acute IFN-I activation can normalize TPO-R signaling, proliferation, and differentiation of Mk-potent stem and progenitor cells (8). Statistical significance indicated as *$P < 0.05$; **$P < 0.01$, ***$P < 0.001$ by Student's *t* test; no asterisk or n.s., not significant.

Provided online are Table S1, Table S2, Table S3, Table S4, Table S5, Table S6, Table S7, Table S8, and Table S9. Table S1 lists patient details (Einstein cohort). Table S2 lists differentially expressed genes in AZA-treated cells vs. control cultures. Table S3 lists genes upregulated after AZA treatment and enriched in GSE15330 GMP vs. MEP. Table S4 lists genes upregulated after AZA treatment and enriched in GSE40666 after IFN-α treatment of CD8 T cells for 90 min. Table S5 lists patient details of a longitudinally collected specimen from FIMM cohort. Table S6 lists genes enriched and positively correlated after AZA treatment in GO (negative regulation of Mk differentiation). Table S7 lists genes enriched and positively correlated post AZA treatment in Hallmark (IFN-α response). Table S8 lists antibodies used in study data. Table S9 lists primers used in this study.